



Magnetic properties of the pseudo one-dimensional Heisenberg spin one-half antiferromagnet acetamidinium tetrachlorocuprate(II)
by Lisa Anne Landenburger

A thesis submitted in partial fulfillment of the requirements for the degree of Master of Science in Physics
Montana State University
© Copyright by Lisa Anne Landenburger (1987)

Abstract:

Magnetic susceptibility measurements of the tetrahedrally coordinated system $[\text{CH}_3\text{C}_9\text{NH}_2]_2\text{CuCl}_4$ (Acetamidinium tetrachloro-cuprate II) made on a vibrating sample magnetometer show it to be a weak pseudo one-dimensional anti-ferromagnet with the dominant exchange, $J_2/k = -2.15\text{K}$, directed along chains of magnetic Cu^{++} ions. A weaker intraplanar exchange, $J_1/k = 0.66$, indicates ferromagnetic ordering between chains. A Curie temperature of -1.6K was measured. Susceptibility data reveal an unexpected double peak at 2.5K and 1.8K suggesting the interesting possibility of two phase transitions corresponding to antiferromagnetic ordering of different sublattice pairs. Consistent with crystallographic data reported by Emerson et al. (in press), these sublattice pairs are formed by two crystallographically distinct distorted tetrahedral CuCl_4 groups linked into chains by intermediate acetamidinium ions. It is proposed that these two inequivalent independent chains form a unique four-sublattice system in which one set of chains order throughout the crystal at 2.5K , followed by a three dimensional ordering at 1.8K . This interpretation is consistent with critical EPR linewidth broadening of two separate resonances at the two reported temperatures. Finally, no evidence for an easy axis was found, however, the possibility of a magneto-structural phase transition occurring at 2600 Oe is presented.

MAGNETIC PROPERTIES OF THE PSEUDO ONE-DIMENSIONAL
HEISENBERG SPIN ONE-HALF ANTIFERROMAGNET
ACETAMIDINIUM TETRACHLOROCUPRATE(II)

by

Lisa Anne Landenburger

A thesis submitted in partial fulfillment
of the requirements for the degree

of

Master of Science

in

Physics

MONTANA STATE UNIVERSITY
Bozeman, Montana

August 1987

MAIN LIB.
N378
L233
Cop. 2

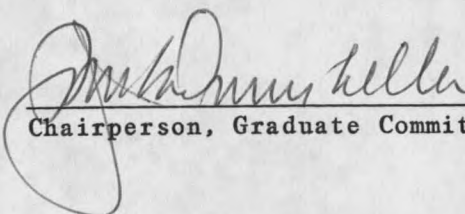
APPROVAL

of a thesis submitted by

Lisa Anne Landenburger

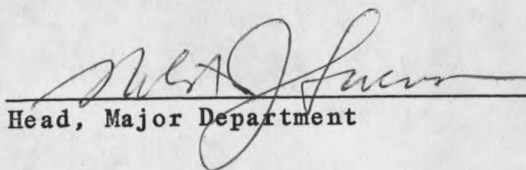
This thesis has been read by each member of the thesis committee and has been found to be satisfactory regarding content, English usage, format, citations, bibliographic style, and consistency, and is ready for submission to the College of Graduate Studies.

26 Aug. 87
Date


Chairperson, Graduate Committee

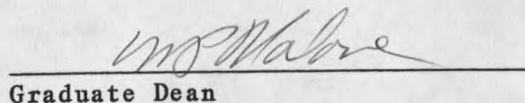
Approved for the Major Department

August 25, 1987
Date


Head, Major Department

Approved for the College of Graduate Studies

9-4-87
Date


Graduate Dean

STATEMENT OF PERMISSION TO USE

In presenting this thesis in partial fulfillment of the requirements for a master's degree at Montana State University, I agree that the Library shall make it available to borrowers under rules of the Library. Brief quotations from this thesis are allowable without special permission, provided that accurate acknowledgment of source is made.

Permission for extensive quotation from or reproduction of this thesis may be granted by my major professor, or in his absence, by the Director of Libraries when, in the opinion of either, the proposed use of the material is for scholarly purposes. Any copying or use of the material in this thesis for financial gain shall not be allowed without my written permission.

Signature

Lisa Anne Landenburg

Date

August 21, 1987

ACKNOWLEDGMENTS

I wish to express gratitude to my advisor, Jack Drumheller, for his support and continued interest in this project. Jerry Rubenacker is warmly acknowledged for his valuable help in the laboratory as well as for the many discussions which helped to shed insight onto this study. Thanks are also due to Ken Emerson of the Department of Chemistry at MSU, for providing the necessary AceTCC crystals and for many enlightening discussions. I am also thankful to John Carlsten and Dick Smith for reviewing the manuscript and making helpful suggestions. Finally, thanks are given to Don Haines for help with the printing of this manuscript. This study was supported by NSF grant DMR-8403993 to Jack Drumheller.

TABLE OF CONTENTS

	Page
1. INTRODUCTION.....	1
2. BACKGROUND.....	4
Theoretical Behavior of Antiferromagnets.....	4
Exchange Interactions.....	4
Susceptibility as a Function of Temperature.....	4
Magnetization as a Function of Field.....	7
Heisenberg Model of Spin Interactions.....	12
Model Description.....	12
High Temperature Series Expansion.....	14
3. METHODOLOGY.....	20
Experimental Apparatus.....	20
Vibrating Sample Magnetometer.....	20
Temperature Control.....	22
Data Acquisition.....	22
Sample Preparation.....	24
Crystal Structure.....	24
4. RESULTS AND DISCUSSION.....	29
Susceptibility Versus Temperature.....	29
Magnetization Versus Angle and Field.....	34
Comparison with EPR Study.....	44
High Temperature Series Expansion.....	47
Comparison with Crystallographic Data.....	49
5. CONCLUSIONS.....	52
REFERENCES CITED.....	54
APPENDIX-- SUPPLEMENTAL SUSCEPTIBILITY PLOTS.....	56

LIST OF FIGURES

Figure	Page
1. Schematic of AceTCC showing a series of tetrahedrally coordinated Cu^{++} ions linked into chains by intermediate acetamidinium ions. An isolated Cu^{++} tetrahedral site is shown in the upper left.....	2
2. Behavior of magnetic susceptibility versus temperature for a typical antiferromagnet.....	6
3. Schematic representation of spin alignment below the Neel temperature for a simple antiferromagnet with two identical interpenetrating sublattices.....	6
4. Anisotropy of an antiferromagnet below the Neel temperature.....	8
5. Behavior of magnetization versus magnetic field applied perpendicular to the easy axis.....	10
6. Behavior of magnetization versus magnetic field applied parallel to the easy axis.....	11
7. Schematic diagram of a vibrating sample magnetometer.....	21
8. Schematic diagram of a vibrating sample magnetometer with an accompanying liquid helium cryostat.....	23
9. Projection of a portion of the crystal structure of AceTCC onto the b-c plane showing an array of site 1 CuCl_4 ions linked into chains parallel to the b-axis by intermediate A4 groups.....	26
10. Projection of a portion of the crystal structure of AceTCC onto the b-c plane showing an array of site 2 CuCl_4 ions linked into chains parallel to the b-axis by intermediate A3 groups.....	27
11. A three dimension representation of the unit cell of AceTCC projected onto the a-b plane.....	28
12. Susceptibility of AceTCC versus temperature at a field strength of 4500 Gauss.....	30

LIST OF FIGURES--Continued

Figure	page
13. Inverse susceptibility versus temperature at a field strength of 4500 Gauss applied parallel to the a-axis.....	31
14. Expanded view of the transition area of figure 11 revealing two separate peaks in the susceptibility.....	33
15. Laboratory coordinate system describing the orientation of an AceTCC crystal in a magnetic field.....	35
16. Angle dependence of magnetization of AceTCC in the a-c plane at 1.75K ($\theta = 90^\circ$; $\phi = 0-360^\circ$).....	36
17. Magnetization versus field at 1.75K ($\theta = 90^\circ$; $\phi = 90^\circ$)....	37
18. Magnetization versus field at 1.75K ($\theta = 90^\circ$; $\phi = 20^\circ$)....	39
19. Magnetization versus field at 1.75K ($\theta = 90^\circ$; $\phi = 45^\circ$)....	40
20. Magnetization versus field at 1.75K ($\theta = 90^\circ$; $\phi = 0^\circ$).....	41
21. Magnetization versus field at 1.9K ($\theta = 90^\circ$; $\phi = 0^\circ$).....	42
22. Magnetization versus field at 3K ($\theta = 90^\circ$; $\phi = 0^\circ$).....	43
23. Magnetization versus field for a powder at 1.75K and 1.9K.....	45
24. Magnetization versus field for a powder at 3K.....	46
25. Magnetic susceptibility data fitted to a high temperature series expansion for a spin 1/2 Heisenberg interaction.....	48
26. A schematic representation of AceTCC showing sheets of site 1 and site 2 copper ions coincident to the b-c plane. Directions of exchange paths are indicated.....	50
27. Expanded view of the transition area for a susceptibility versus temperature scan taken at 4000 Gauss.....	57
28. Expanded view of the transition area for a susceptibility versus temperature scan taken at 2000 Gauss.....	58
29. Expanded view of the transition area for a susceptibility versus temperature scan taken at 4500 Gauss.....	59

ABSTRACT

Magnetic susceptibility measurements of the tetrahedrally coordinated system $[\text{CH}_3\text{C}(\text{NH}_2)_2]_2\text{CuCl}_4$ (Acetamidinium tetrachlorocuprate II) made on a vibrating sample magnetometer show it to be a weak pseudo one-dimensional anti-ferromagnet with the dominant exchange, $J_2/k = -2.15\text{K}$, directed along chains of magnetic Cu^{++} ions. A weaker intraplanar exchange, $J_1/k = 0.66$, indicates ferromagnetic ordering between chains. A Curie temperature of -1.6K was measured. Susceptibility data reveal an unexpected double peak at 2.5K and 1.8K suggesting the interesting possibility of two phase transitions corresponding to antiferromagnetic ordering of different sublattice pairs. Consistent with crystallographic data reported by Emerson et al. (in press), these sublattice pairs are formed by two crystallographically distinct distorted tetrahedral CuCl_4 groups linked into chains by intermediate acetamidinium ions. It is proposed that these two inequivalent independent chains form a unique four-sublattice system in which one set of chains order throughout the crystal at 2.5K , followed by a three dimensional ordering at 1.8K . This interpretation is consistent with critical EPR linewidth broadening of two separate resonances at the two reported temperatures. Finally, no evidence for an easy axis was found, however, the possibility of a magneto-structural phase transition occurring at 2600 Oe is presented.

CHAPTER ONE

INTRODUCTION

Motivation to study magnetic properties of acetamidinium tetrachlorocuprate (II), $[\text{CH}_3\text{C}(\text{NH}_2)_2]_2\text{CuCl}_4$, herein referred to as AceTCC, originated in the search for the rare and elusive one dimensional, spin 1/2 Heisenberg ferromagnet (1D 1/2 HF). Cause for this search is based on the successful observation of bound magnons in these scarce systems (Hoogerbeets et al., 1984; Haines et al., 1987). Synthesis of new (1D 1/2 HF) compounds and characterization of their magnetic properties will enable further experiments to be carried out with the prospects of obtaining a more comprehensive understanding of bound magnons. A structural model of AceTCC proposed by Bares, et al. (1969) based on x-ray crystallographic analysis, suggests that the system consists of chains of tetrahedrally-coordinated copper ions with intermediate acetamidinium ions forming a bridge through which magnetic exchange may most likely occur. Figure 1 shows a schematic of the atomic structure of these chains. It was originally thought that this exchange interaction may be strong only along the chain (i.e., one dimensional) and ferromagnetic in behavior— hence, the incentive for investigation. Susceptibility measurements made on a vibrating sample magnetometer, however, reveal that the system is in fact antiferromagnetic. Although the one-dimensional ferromagnet was not found, results of the measurements of AceTCC disclose some unexpected

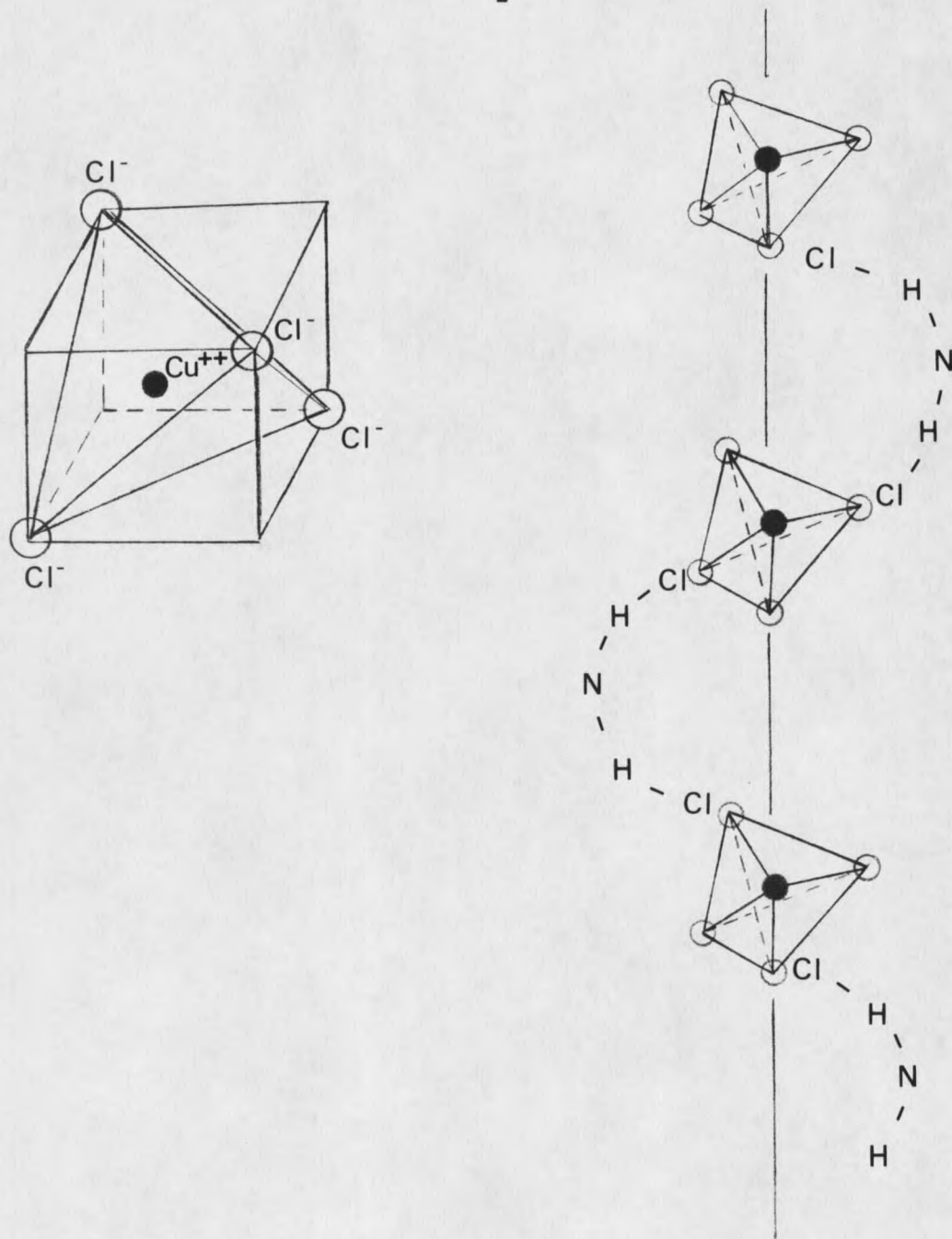


Figure 1. Schematic of $[\text{CH}_3\text{C}(\text{NH}_2)_2]_2\text{CuCl}_4$ showing a series of tetrahedrally coordinated Cu^{++} ions linked into chains by intermediate acetamidinium ions. An isolated Cu^{++} tetrahedral site is shown in the upper left.

and interesting properties, significant enough that continued investigation was warranted. Characterization of these and other newly observed magnetic properties form the basis of this investigation and are reported and discussed below.

CHAPTER TWO

BACKGROUND

Theoretical Behavior of AntiferromagnetsExchange Interactions

The magnetic moment of an ion is a consequence of the spin and orbital motion of its electrons. The main magnetic features characteristic of ferro-, ferri- and antiferromagnetic materials are produced by coupling between these magnetic moments in a solid. The mechanism responsible for this coupling lies in the exchange effects due to overlap of atomic wavefunctions. In particular, the magnitude of exchange is a direct function of the overlap and thus measures the extent to which magnetic spins and dipole moments of nearby electrons are correlated. In antiferromagnets, exchange energy is minimized when neighboring atomic moments are aligned antiparallel to one another.

Susceptibility as a Function of Temperature

Alignment of magnetic spins can occur only when the interaction energy is large enough to compete with thermal vibrational energy of the system. Thus, as the temperature of an antiferromagnet is gradually lowered, a critical temperature known as the Neel temperature, T_N , is reached where exchange energy begins to compete with and overcome thermal energy. This temperature marks the

transition from a non-ordered (paramagnetic) state to an ordered antiferromagnetic state. This is illustrated most clearly in a plot of magnetic susceptibility against temperature as shown in Figure 2. The resulting characteristic temperature scan of an antiferromagnet shows the susceptibility increasing with decreasing temperature until it passes through a maximum at a temperature slightly above the Neel temperature. It should be pointed out that the transition does not correspond exactly to the maximum susceptibility, but rather to the point of maximum increasing slope (Lasheen, et al., 1958; Fisher, 1962). Well above T_N , the system behaves paramagnetically according to the Curie-Weiss law:

$$\chi = C/(T-\theta),$$

where C and θ are called the Curie constant and Curie temperature respectively.

Below T_N , the system falls into an ordered state such that adjacent magnetic moments align antiparallel to one another. For convenience one can consider the magnetic moments to lie on two similar interpenetrating sublattices, within each of which, the moments are all parallel to one another yet antiparallel to those in neighboring sublattices as shown in Figure 3. At absolute zero, alignment is complete and net magnetization of the system is zero.

Often, a strong anisotropy below the Neel temperature is evident in antiferromagnets. Depending on the direction of the applied field relative to a given crystallographic axis, the susceptibility behaves differently. For antiferromagnets there often exists a preferred

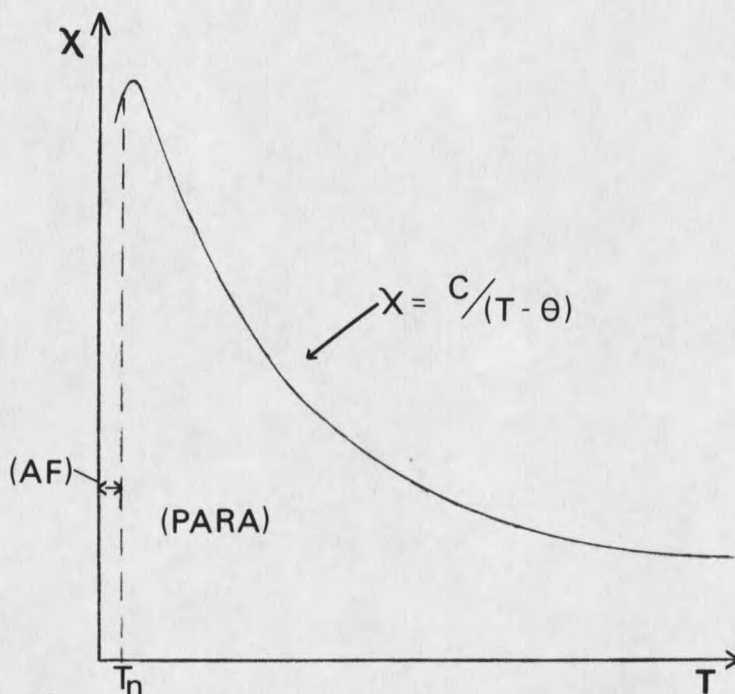


Figure 2. Behavior of magnetic susceptibility versus temperature for a typical antiferromagnet. Above T_N the system behaves paramagnetically in accordance to the Curie-Weiss law. Below T_N the system is in an ordered antiferromagnetic state.

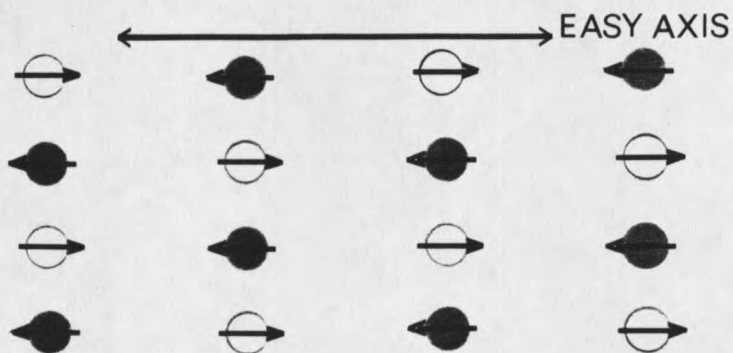


Figure 3. Schematic representation of spin alignment below the Neel temperature for a simple antiferromagnet with two identical interpenetrating sublattices. Magnetic spins on one sublattice (ie, dark circles) are all parallel to each other yet antiparallel to spins on the neighboring sublattice (light circles).

direction, called the easy axis or the spin direction, along which the spins tend to align in the absence of an external magnetic field. It is instructive to consider two cases: 1) H perpendicular and 2) H parallel to the easy axis. When a constant field, H , is applied in a direction perpendicular to the easy axis, the magnetic moments on both sublattices will rotate toward H by equal amounts. The susceptibility in this direction, χ , was calculated by Van Vleck (1941) for temperatures below T_N and shown to be independent of temperature with a constant value of $C/2\theta$. However, if instead, the applied field is directed parallel to the easy axis, something very different occurs. Assuming absolute zero and thus, perfect ordering, application of a weak field (weaker than some critical value) parallel to the spin direction is not sufficient to rotate the spins from the easy axis. Thus, no net moment is generated, and at absolute zero, χ will be zero. However, even a slight increase in temperature will introduce enough thermal noise to generate small disordering fluctuations, small rotations of the magnetic spins, and hence, a small susceptibility. As the temperature continues to climb toward the transition temperature, the alignment becomes increasingly disordered until χ matches χ at T_N . This is illustrated in Figure 4.

Magnetization as a Function of Field

More insight into this apparent anisotropy is gained by considering the behavior of an antiferromagnet in a changing magnetic field. Again, consider H perpendicular and H parallel to the easy axis. In both cases it is assumed that a constant temperature well

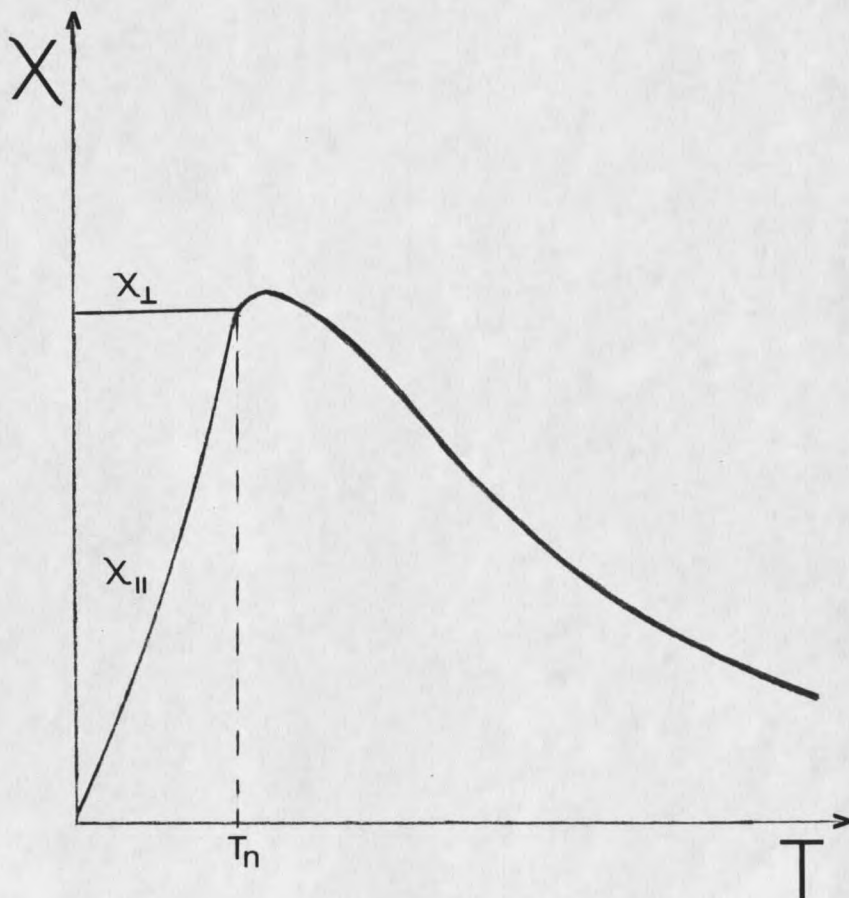


Figure 4. Anisotropy of an antiferromagnet below the Neel temperature. χ_{\parallel} and χ_{\perp} are the magnetic susceptibilities parallel and perpendicular to the easy axis of the crystal.

below T_N is maintained. With H applied perpendicular to the easy axis, the magnetic moments will again tend to rotate toward H , causing magnetization to increase linearly with field strength. Eventually saturation is achieved, resulting in alignment of the magnetic moments parallel to the external field. This is illustrated in Figure 5.

Consider now H directed along the easy axis. Since χ is greater than χ for an antiferromagnet below the Neel temperature, it would be more energetically favorable for the spin direction to be at right angles to H . Although one might expect the coupled magnetic spins to rotate toward this perpendicular orientation, Nagamiya (1951) determined that crystal anisotropy forces oppose this rotation and strongly couple the spins to the easy axis. If an external field, weaker than the anisotropy field, is applied along the easy axis, nothing happens and the net magnetization of the system remains zero. If, however, the external field strength is increased sufficiently, a critical value H_C , is reached where the field strength overcomes these anisotropy forces and the spins 'flop' to a near right angle from the easy axis. As shown in Figure 6, this sharp (first order) transition to the spin-flop phase is characterized by a sudden increase in magnetization. As the field strength continues to increase beyond H_C , a smooth second order transition takes the system into a saturated paramagnetic state.

This anisotropy, characterized by a preferred direction of alignment in the absence of a field, may be due to many contributing effects such as spin-orbit coupling, ligand field effects, and (or) dipolar interactions. Regarding the anisotropy as a fictitious

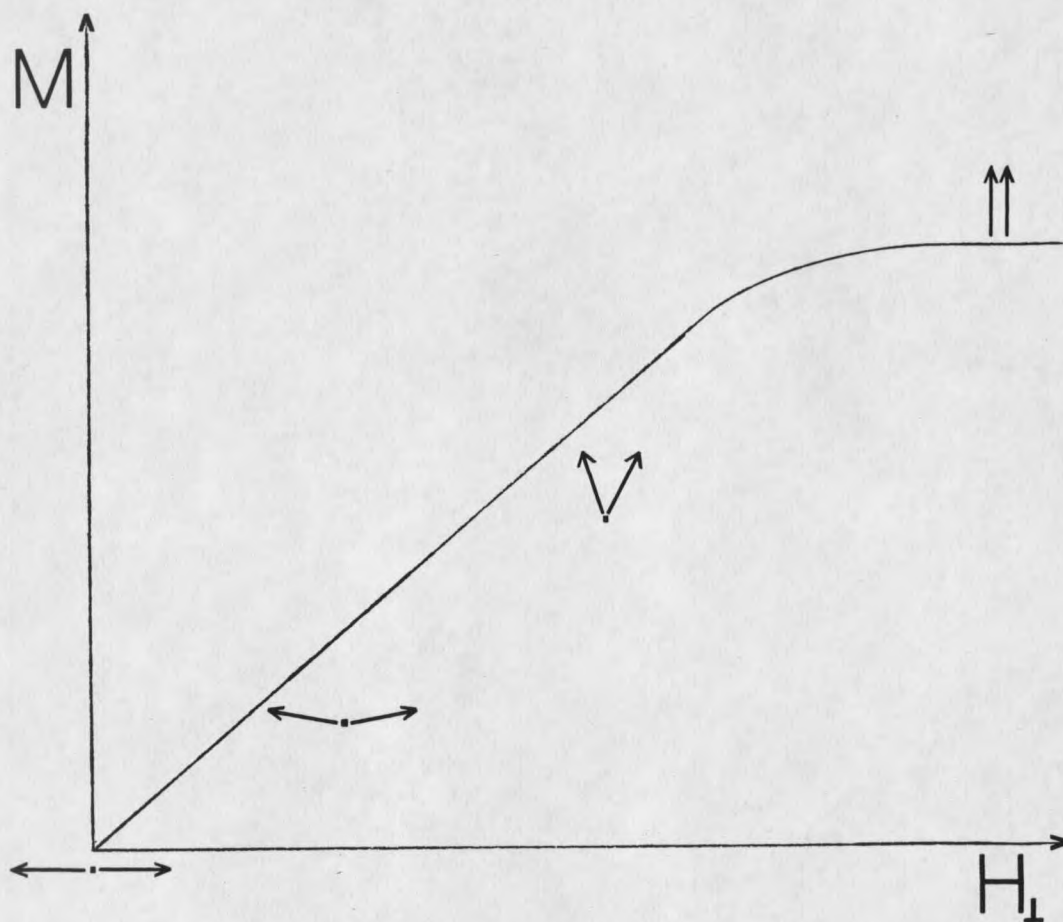


Figure 5. Behavior of magnetization versus magnetic field applied perpendicular to the easy axis. Arrows represent relative alignment of spins from two different sublattices.

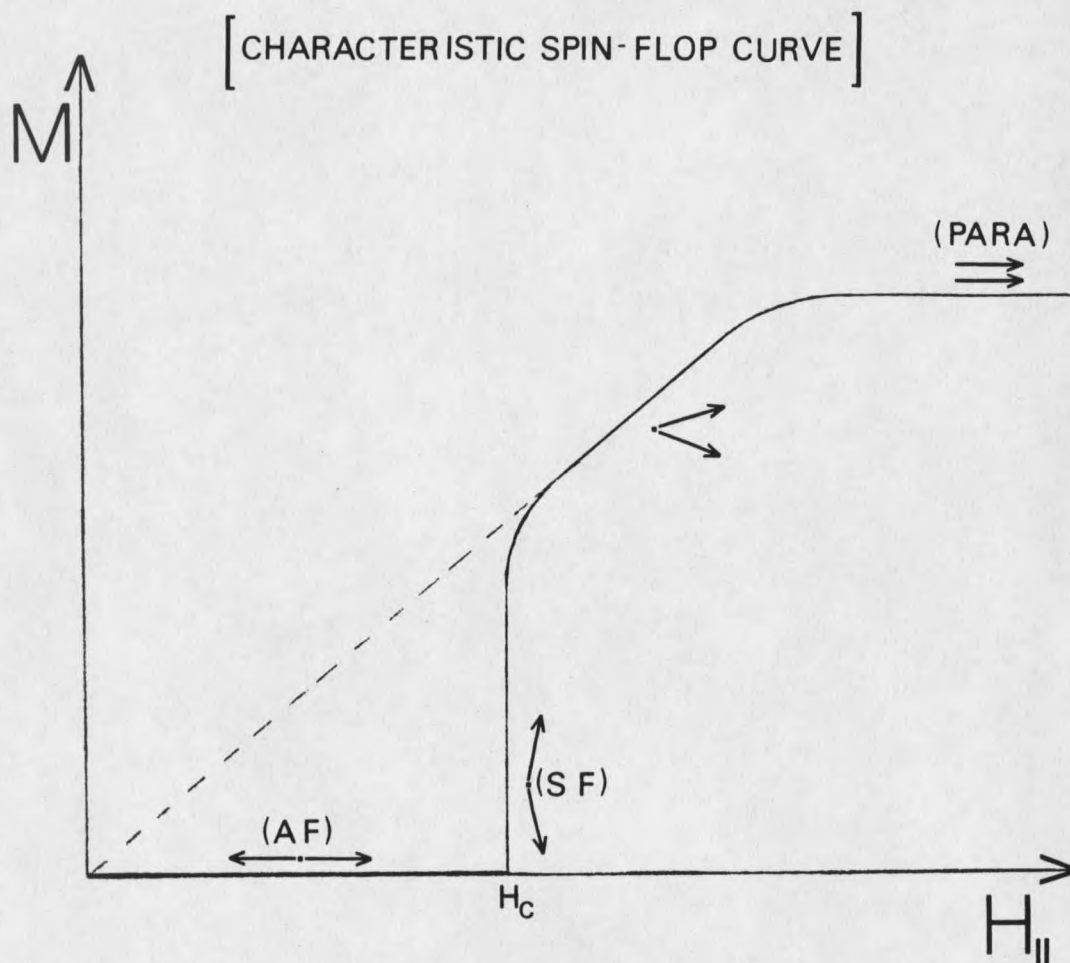


Figure 6. Behavior of magnetization versus field applied parallel to the easy axis. At H_C the field strength overcomes the competing anisotropy and induces a first order transition from the antiferromagnetic (AF) phase to the spin-flop (SF) phase. Magnetization then increases linearly with field until a saturated paramagnetic (PARA) state is achieved.

internal field H_A , the critical spin-flop field can be found from

$$H_C = (2H_E H_A)^{1/2}$$

where H_E is the measured antiferromagnetic exchange energy, J/k, converted to units of Gauss (Martin, 1967). Typically $H_E \gg H_A$. For many antiferromagnets H_E is of the order 10^6 Gauss while H_A is typically of the order 10^2 to 10^3 Gauss.

Heisenberg Model of Spin Interactions

Model Description

The spontaneous magnetization observed at low temperatures is a direct consequence of exchange interactions between magnetic ions. Theoretical analysis of this phenomenon rests on the proper choice of a model to yield a plausible description of these interactions. It was first proposed by P. Weiss (1907) that the observed spontaneous magnetization was the result of dipole-dipole interactions. However, dipolar interactions have been shown to be much too small to account for the high transition temperatures observed in many ferromagnetic materials (Rosenberg, 1983, p.196). Instead, Heisenberg (1926; 1928) showed that the exchange interactions are a manifestation of the restraints placed on the electronic wavefunctions by the Pauli exclusion principle. More specifically, the requirement that the wavefunctions of an electron pair be antisymmetric with respect to exchange of their space and spin coordinates, directly affects the alignment of the magnetic spins and hence the magnetic dipole moments. The effect of the exclusion principle is to separate electrons with

parallel spins and therefore to minimize their mutual Coulomb repulsion. The resulting energy eigenvalues depend heavily on the specific electrostatic (Coulomb) forces at play within the solid, which in turn govern the spin configuration in accordance to the Pauli principle.

The most generally accepted model representing the Coulomb interactions responsible for ordering is the Heisenberg Hamiltonian

$$H = -2 \sum_{ij} J_{ij} \bar{S}_i \cdot \bar{S}_j$$

where the sum is over all lattice sites i and j . J_{ij} is the exchange integral (coupling constant) between neighboring ions, and \bar{S}_i and \bar{S}_j are the resultant spin moments associated with ions i and j . Underlying the Heisenberg model is the assumption that in a crystal field the orbital momenta are nearly quenched so that magnetic interactions may be represented as almost pure spin-spin interactions. Additionally it is assumed that the magnetic ions are localized at identical lattice sites throughout the sample. Note that when the coupling constant J is negative, the Heisenberg Spin Hamiltonian favors an antiparallel (antiferromagnetic) alignment between adjacent spins on opposite sublattices, and thus minimum energy. A positive value of J indicates a parallel (ferromagnetic) alignment of adjacent spins. Furthermore, the difference in energy between the parallel and antiparallel spin configurations is simply equal to the exchange energy for spin $1/2$ particles. The general use of the Heisenberg model is founded on its success at, amongst other things, accounting for spin waves and its agreement with Hund's rules and the Pauli exclusion

principle.

High Temperature Series Expansion

With the Heisenberg model in hand it is possible to determine the magnitude of the inter-ionic exchange coupling, J , between electrons in a solid. An exact solution however, is not possible since diagonalization of the Hamiltonian is exceedingly complex. Instead, one relies on model fitting. Since many thermodynamic properties of a system are easily determined once the appropriate partition function, Z , is known, one expands Z as a series in powers of $1/kT$ and evaluates coefficients of the first few terms for Heisenberg interactions. Expressing magnetic susceptibility in terms of Z , and treating J as a parameter, susceptibility data are then fitted to this high temperature series expansion. The best fit corresponds to the theoretical value for J . This high temperature series expansion theory for a spin $1/2$ system is examined here and follows the format provided by Martin (1967).

Consistent with the theory of statistical mechanics, the partition function for a system at an equilibrium temperature T , is defined as

$$Z = \sum_c \exp(- E_c/kT)$$

where k is the Boltzmann constant and E_c is the energy of the c -th excited state; each state corresponding to a distinct spin configuration. It can then be shown (Kittel, 1958, p.85) that the volume susceptibility for a sample of volume V , is given as

$$\chi_v = (kT/V) \partial^2 (\ln Z) / \partial H^2$$

where H is the external field strength. Note that, with temperature, an ordered spin configuration is increasingly disturbed and the system undergoes random transitions into and out of the many possible states. Consequently, construction of magnetic susceptibility in terms of the partition function accounts for a thermal average of these fluctuating energy exchanges.

Defining β as $1/kT$, the exponential function in Z can be expressed as a series in powers of β .

$$\begin{aligned} Z &= \sum_c [1 - \beta E_c + \beta^2 (E_c^2/2!) - \beta^3 (E_c^3/3!) + \dots] \\ &= N_s - \beta \sum_c (E_c) + \beta^2 \sum_c (E_c^2/2!) - \beta^3 \sum_c (E_c^3/3!) + \dots \end{aligned}$$

where N_s is the total number of accessible states. It is convenient to define the mean-value

$$\bar{E}^n = \sum_c E_c^n / N_s$$

so that the series can be written as

$$Z/N_s = 1 - \beta \bar{E} + (\beta^2/2!) \bar{E}^2 - (\beta^3/3!) \bar{E}^3 + \dots$$

Taking the natural log of both sides and expanding the right hand side gives

$$\begin{aligned} \ln(Z/N_s) &= [-\beta \bar{E} + (\beta^2/2!) \bar{E}^2 - \dots] - [-\beta \bar{E} + (\beta^2/2!) \bar{E}^2 - \dots]^2 \\ &\quad + [-\beta \bar{E} + (\beta^2/2!) \bar{E}^2 - \dots]^3 + \dots \end{aligned}$$

The terms with like powers of β can be combined to give the following

series

$$\ln(Z/N_s) = -\bar{E}\beta + (\bar{E}^2 - \bar{E}^2)\beta^2/2! - (\bar{E}^3 - 3\bar{E}^2\bar{E} + 2\bar{E}^3)\beta^3/3! + \dots$$

Since thermodynamic properties, such as susceptibility and magnetization, are proportional to N , all terms of higher order in N must cancel. Therefore, the series can be simplified by writing

$$\ln(Z/N_s) = -\bar{E}_N\beta + \bar{E}_N^2(\beta^2/2!) - \bar{E}_N^3(\beta^3/3!) + \dots$$

where \bar{E}_N^n includes only those terms of first order in N .

Up until this point the results obtained have been completely general and independent of the type of interaction between the magnetic ions of the system. Specification of the interaction type however, allows one to evaluate the mean-value coefficients \bar{E}_N , \bar{E}_N^2 , \bar{E}_N^3 etc. in such a way that a precise knowledge of the energy eigenstates is not necessary. As an example, consider a solid in which the exchange interaction is very weak except between nearest neighbors. As discussed on page , the Heisenberg exchange interaction for a single ion is

$$H = -2 \sum_j J_{ij} \bar{S}_i \cdot \bar{S}_j$$

where the summation is over nearest neighbors. Summing over all ions in the crystal, the Hamiltonian for the total system is given as

$$H = -2 \sum_{ij} J_{ij} (S_{ix}S_{jx} + S_{iy}S_{jy} + S_{iz}S_{jz})$$

For the purpose of illustration, assume a special case of the Heisenberg model known as the Ising interaction. The spin quantization in this case is along a preferred direction, defined for convenience

as the z-axis, so that

$$H^I = -2 \sum_{ij} S_{iz} S_{jz} .$$

Although very few solids are represented accurately by the Ising model, its main advantage is that thermodynamic quantities of one and two dimensional systems can be determined exactly (Newell and Montroll, 1953). In the presence of an external field, the Hamiltonian contains a Zeeman interaction term in addition to the above spin-spin coupling. Application of the Ising Hamiltonian for this spin 1/2 system allows the computation of the first mean-value coefficient.

$$\begin{aligned} E &= \sum_c E_c / N_s \\ &= \sum_c \sum_{i=1}^N [-2JS_{iz}S_{(i+1)z} - \mu_B g H_z S_{iz}] \end{aligned}$$

where the summation is over all N ions in the sample. Here, μ_B is the Bohr magnon and g is the Lande factor.

For a given spin there are $N_s N/4$ states corresponding to each of the following energies.

$$E = (-J - \mu_B g H) / 2$$

$$E = (+J - \mu_B g h) / 2$$

$$E = (+J + \mu_B g h) / 2$$

$$E = (-J + \mu_B g h) / 2$$

Summing over all spins from $i=1$ to N , each energy value occurs an equal number of times and thus cancel one another. The result is zero for the first coefficient.

$$\bar{E} = 0$$

Due to invariance of the Hamiltonian trace, one can expand the second coefficient as follows

$$\begin{aligned}\overline{E^2} &= (1/N_s) \sum_c \sum_{i=1}^N [4J^2 S_{iz}^2 S_{(i+1)z}^2 + \mu_B^2 g^2 H^2 S_{iz}^2] \\ &= N(J^2 + \mu_B^2 g^2 H^2)/4\end{aligned}$$

Plugging these results of the first two expansion coefficients into the partition function expansion gives

$$\ln(Z/N_s) = N\beta^2 (J^2 + \mu_B^2 g^2 H^2)/8 + \theta(\beta^3) + \dots$$

Recalling that volume susceptibility is defined as

$$\begin{aligned}\chi_V &= (kT/V) \partial^2 (\ln Z) / \partial H^2 \\ &= (kT/V) \partial^2 (\ln Z/N_s) / \partial H^2\end{aligned}$$

we then have

$$\chi_V = (N\mu_B^2 g^2) / (4VkT) + \theta(\beta^2) + \dots$$

Proceeding in the same manner and keeping only those terms proportional to the first power of N , the series for an Ising spin 1/2 system becomes

$$\chi_V = (N\mu_B^2 g^2) / (4VkT) [1 + (J/kT)/2 + (J/kT)^2/8 + \dots]$$

Although the above series was evaluated for an Ising interaction, the method illustrated is the same for the more complicated Heisenberg interaction. However, the Heisenberg model assumes no preferred axis for spin quantization, consequently, the vector product $\vec{S}_i \cdot \vec{S}_j$ makes

the computations exceedingly involved. Calculations for various spin values and lattice types have been carried out to six or seven terms by Van Dongen et al. (1925), Rushbrooke and Wood (1958), and by Domb and Sykes (1962). Other valuable work has been completed by P. Seifert, but due to an untimely death, has never been published. The series expansion used for fitting to susceptibility data generated in this current study is based on the work of P. Seifert and is quoted below in terms of the Curie-Weiss θ and of ε , a measure of deviation from a square planar magnetic lattice

$$\begin{aligned} \chi_V = (C/T) [& 1 + \theta/T + (\theta/T)^2/2 (1 - 2\varepsilon - 3\varepsilon^2) + \\ & + (\theta/T)^3/6 (1 - 9\varepsilon - 15\varepsilon^2 - 3\varepsilon^3) + \\ & + 13(\theta/T)^4/192 (1 - 15.8\varepsilon - 16.2\varepsilon^2 + 28.6\varepsilon^3 + 31.2\varepsilon^4)] \end{aligned}$$

The parameters θ and ε in the above series can be written in terms of an intraplanar coupling constant J_1 and a linear coupling constant J_2 as follows

$$J_1 = (1 + \varepsilon)\theta/2$$

$$J_2 = -\theta\varepsilon/2.$$

Note that if $\varepsilon = 0$, then $J_2 = 0$. In this case there is no coupling between planes, and the model corresponds to an ideal two dimensional system. Likewise, if $\varepsilon = -1$ then $J_1 = 0$. In this latter case coupling is restricted to chains, and the model corresponds to an ideal one dimensional system.

CHAPTER THREE

METHODOLOGY

Experimental ApparatusVibrating Sample Magnetometer

Susceptibility and magnetization measurements were taken on a Princeton Applied Research model 155 vibrating sample magnetometer (VSM). A schematic is shown in Figure 7. Here, the sample is mounted at the end of a rod, the other end of the rod being fixed to a mechanical vibrator. The sample end of the rod is lowered between the pole faces of a magnet, allowing both the rod and sample to vibrate at a frequency of 80 hertz with an amplitude of about 0.1mm in a direction perpendicular to the uniform magnetic field. In the presence of this field the sample acquires a magnetic moment, which by virtue of its vibration, induces an alternating emf in two pickup coils mounted on the magnet pole faces. Equipped with a capacitor plate assembly near the top of the vibrating rod, the VSM generates a reference signal against which the sample's signal is compared. A differential amplifier, passing only the differences between the two signals, causes the measurement to be independent of any fluctuations in vibrational amplitude or frequency. This ac difference signal is proportional to the magnetic moment of the sample. The system, which makes bulk measurements averaged over the entire volume of the sample,

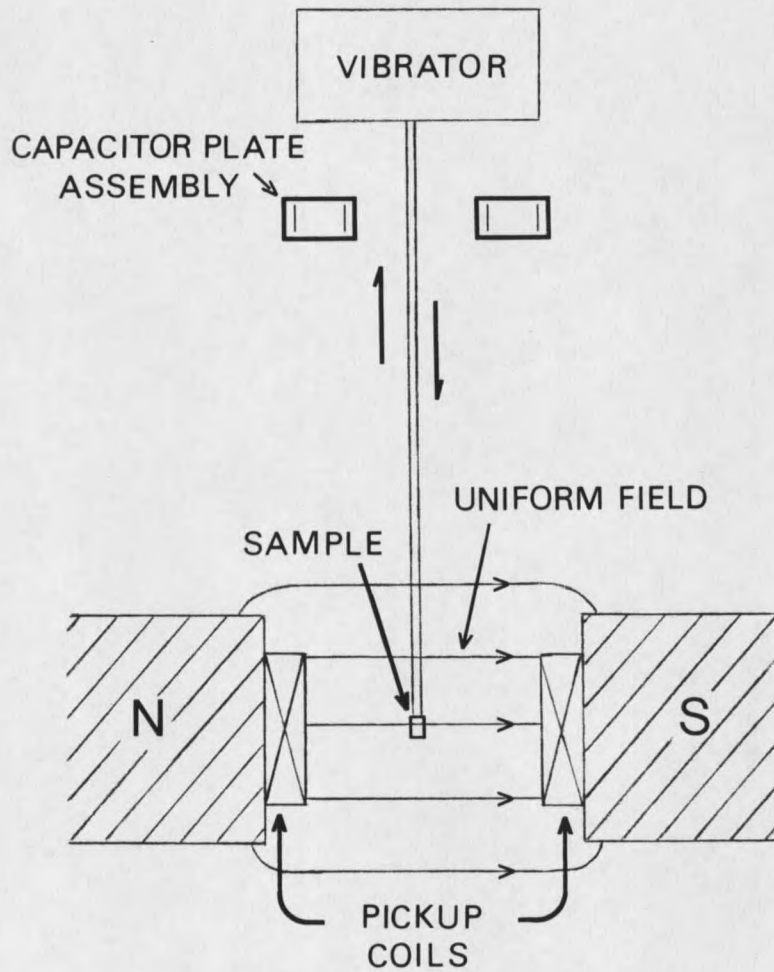


Figure 7. Schematic diagram of a vibrating sample magnetometer (modified from Cullity, p. 67).

can detect a minimum change in magnetic moment of 5×10^{-5} emu per Oersted. This corresponds to a change in magnetic susceptibility of 1×10^{-8} emu for 1cc sample in a field of 5000 Gauss.

Temperature Control

The sample temperature is regulated by a Janus model 153 variable temperature cryostat in which a flow of liquid helium vapor through the sample chamber may be established. By controlling flow rate and temperature of the helium vapor, the sample temperature can be varied over a range of about 4.5K to 300K with a stability greater than .01K. To obtain temperatures below the helium lambda point, the sample chamber can be pumped so that the vapor pressure, and hence, the temperature is lowered. Use of a model 1397 Welsh Scientific pump with a pumping speed of 500 liters per minute yields temperatures down to 1.9K. A second pump installed parallel with the first makes it possible to obtain temperatures as low as 1.5K and to maintain temperatures as low as 1.8K. Temperature is measured by a calibrated carbon glass resistor (CGR) which resides directly above the sample. A schematic of the cryostat in conjunction with the VSM is shown in Figure 8.

Data Acquisition

Data acquisition is accomplished with the aid of a model 455 digital interface coupled to the VSM, and via an IEEE-488 parallel link which establishes two-way communications between the interface console and an Apple IIe computer. This allows the transfer of data

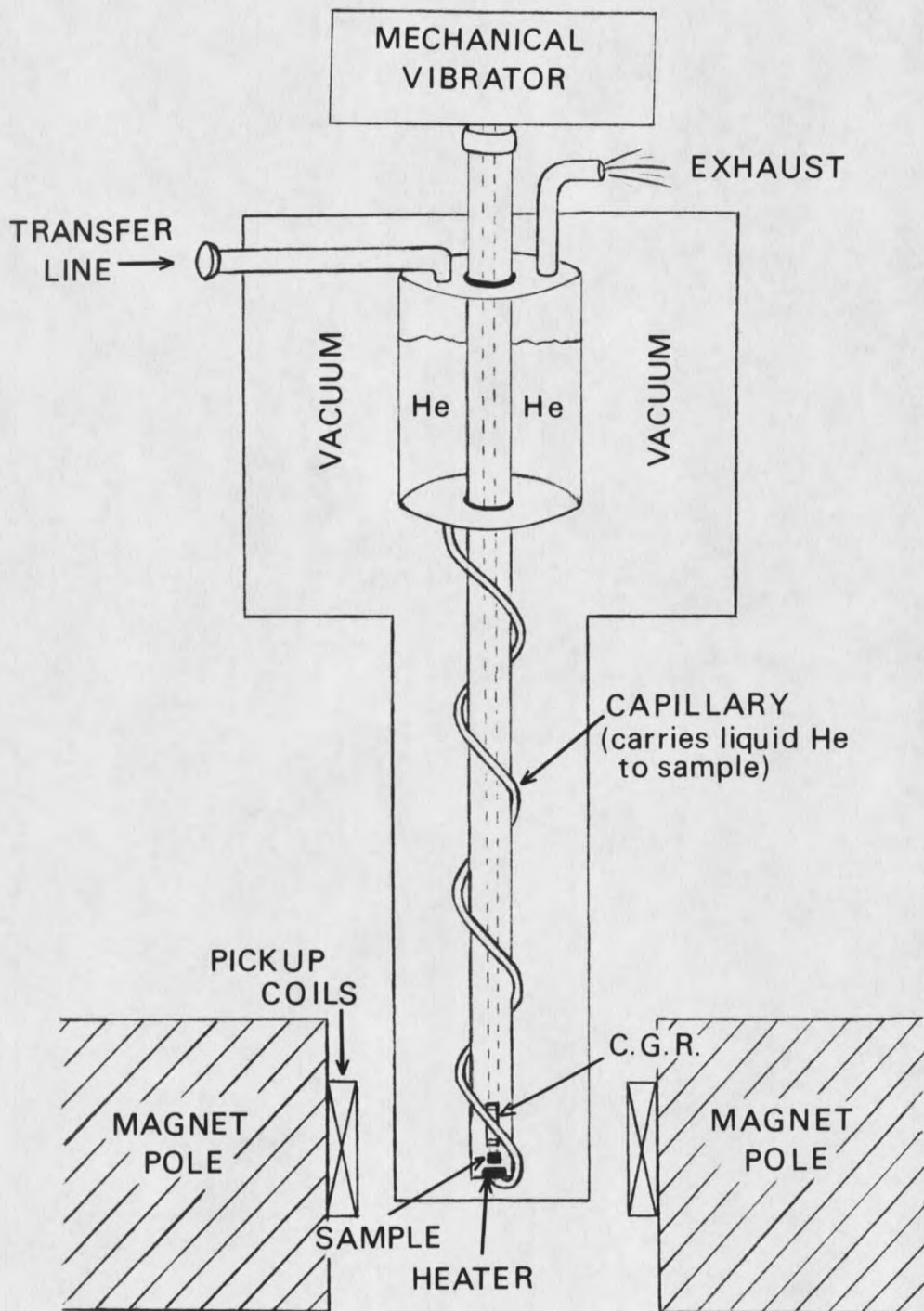


Figure 8. Schematic diagram of a vibrating sample magnetometer with an accompanying liquid helium cryostat.

from the VSM pickup coils to the Apple IIe where the data can then be stored, displayed graphically, and (or) printed out. The above accessories also provide computer control of both the magnetometer power supply and current through the heater element for automatic control of the magnetic field scans and the helium vapor.

Sample Preparation

AceTCC was prepared by mixing stoichiometric amounts of acetamidinium chloride and anhydrous copper(II) chloride in dry alcohol. Crystal precipitation was induced by placing the resultant solutions into a dessicator over diethyl ether, allowing for a slow condensation of ether into the solution. Crystal samples were graciously provided by K. Emerson, professor of Chemistry at MSU.

Crystal Structure

AceTCC consists of two crystallographically distinct tetrahedrally-coordinated CuCl_4 groups which are linked, via intermediate acetamidinium ions, into separate chains parallel to the b-axis (Emerson et al., in press). These two distinct CuCl_4 sites differ only in their associated hydrogen bond networks and in the orientation of their tetrahedral planes. Crystallography measurements indicate that the two tetrahedral axes are mutually separated by an angle of 20° .

Analysis of crystallographic data has also revealed four distinct acetamidinium groups, which if isolated in space, are virtually indistinguishable. However, differences in their neighboring atomic

environments result in slightly different hydrogen bonding. These four acetamidinium groups are the necessary links bridging the two CuCl_4 groups into chains and serve as the bridge connecting the chains into sheets and the sheets, in turn, into a three dimensional system. Figure 9 shows the hydrogen bonding which links a set of site 1 CuCl_4 ions in the b-c plane. The three groups labeled A1, A2 and A3, represent three different acetamidinium groups projected onto the b-c plane. For comparison, the bonding which links the CuCl_4 ions of site 2 is shown in Figure 10. In both figures, the box marks the boundaries of the unit cell. Figure 11 shows an edge-on view of the b-c plane with the hydrogen bonding omitted for clarity. Acetamidinium groups, A4 and A3, link site 1 and site 2 CuCl_4 ions, respectively, into separate chains parallel to the b-axis. The acetamidinium groups, A1 and A2, link these chains into sheets coincident to the a-b plane and form a weak bridge connecting these planar arrays of copper ions into a three dimensional system.

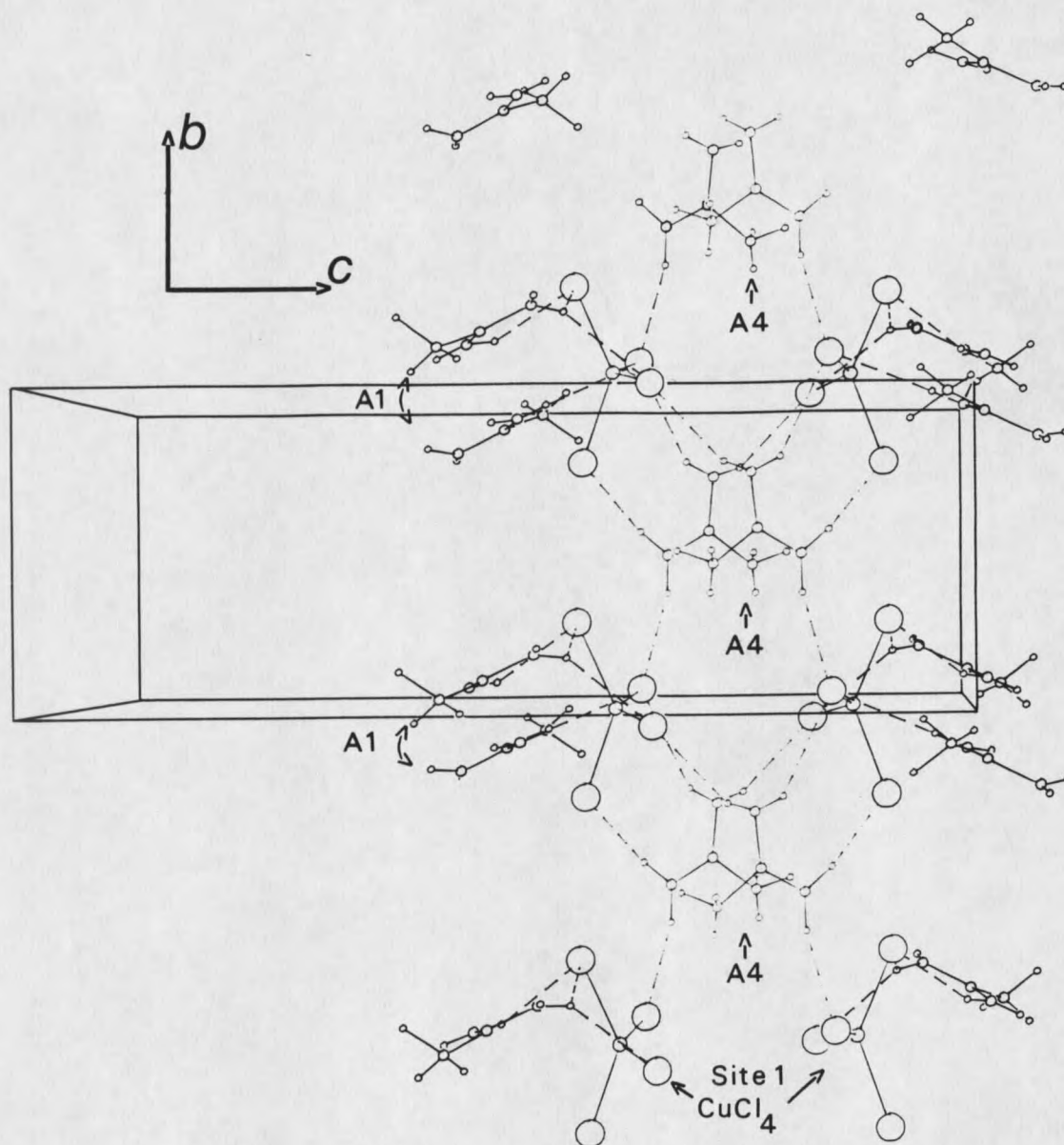


Figure 9. Projection of a portion of the crystal structure of AceTCC onto the b - c plane showing an array of site 1 CuCl_4 ions linked into chains parallel to the b -axis by intermediate A4 groups. A1 and A4 represent two crystallographically distinct acetamidinium ions.

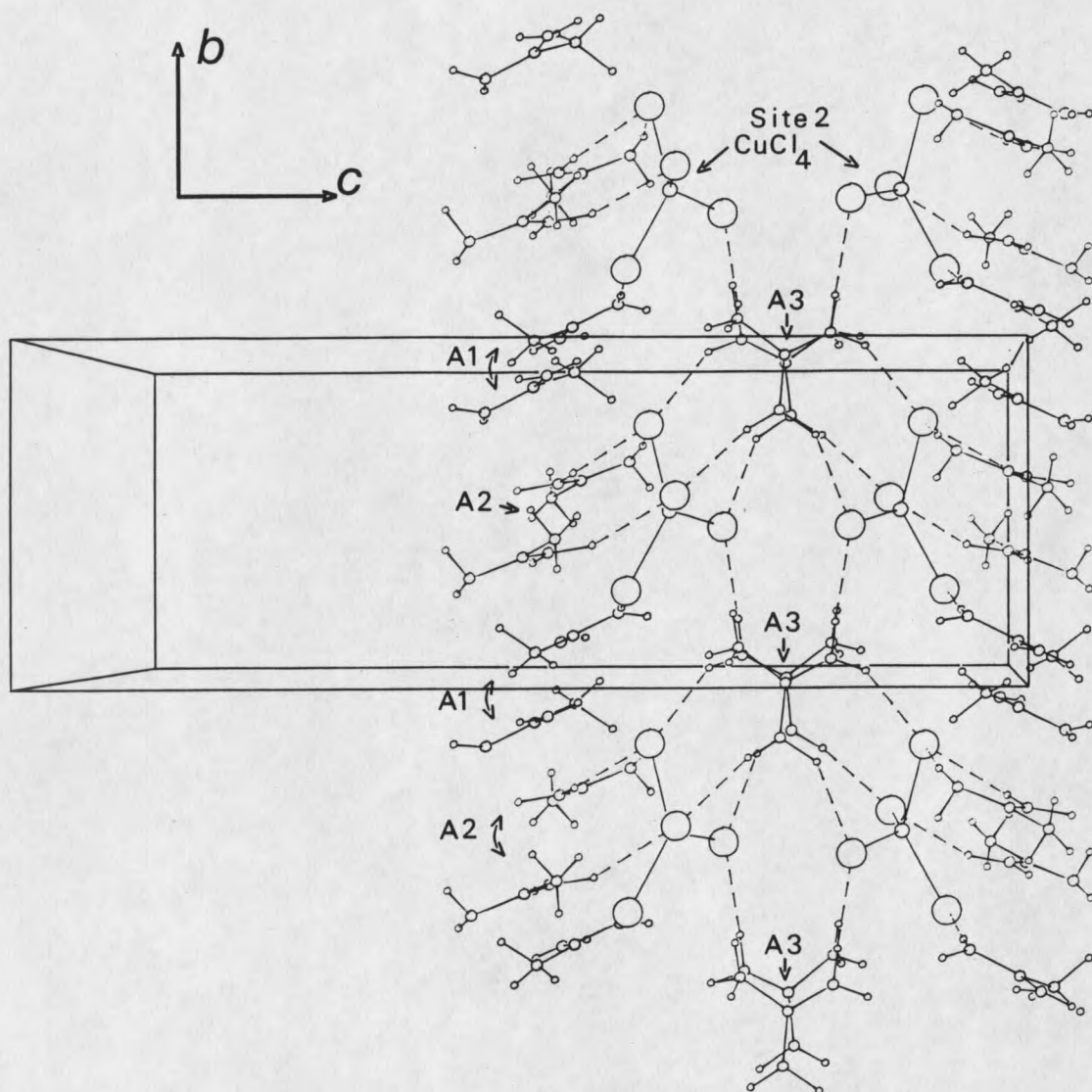


Figure 10. Projection of a portion of the crystal structure of AceTCC onto the b-c plane showing an array of site 2 CuCl_4 ions linked into chains parallel to the b-axis by intermediate A3 groups. A1, A2 and A3 represent three crystallographically distinct acetamidinium ions.

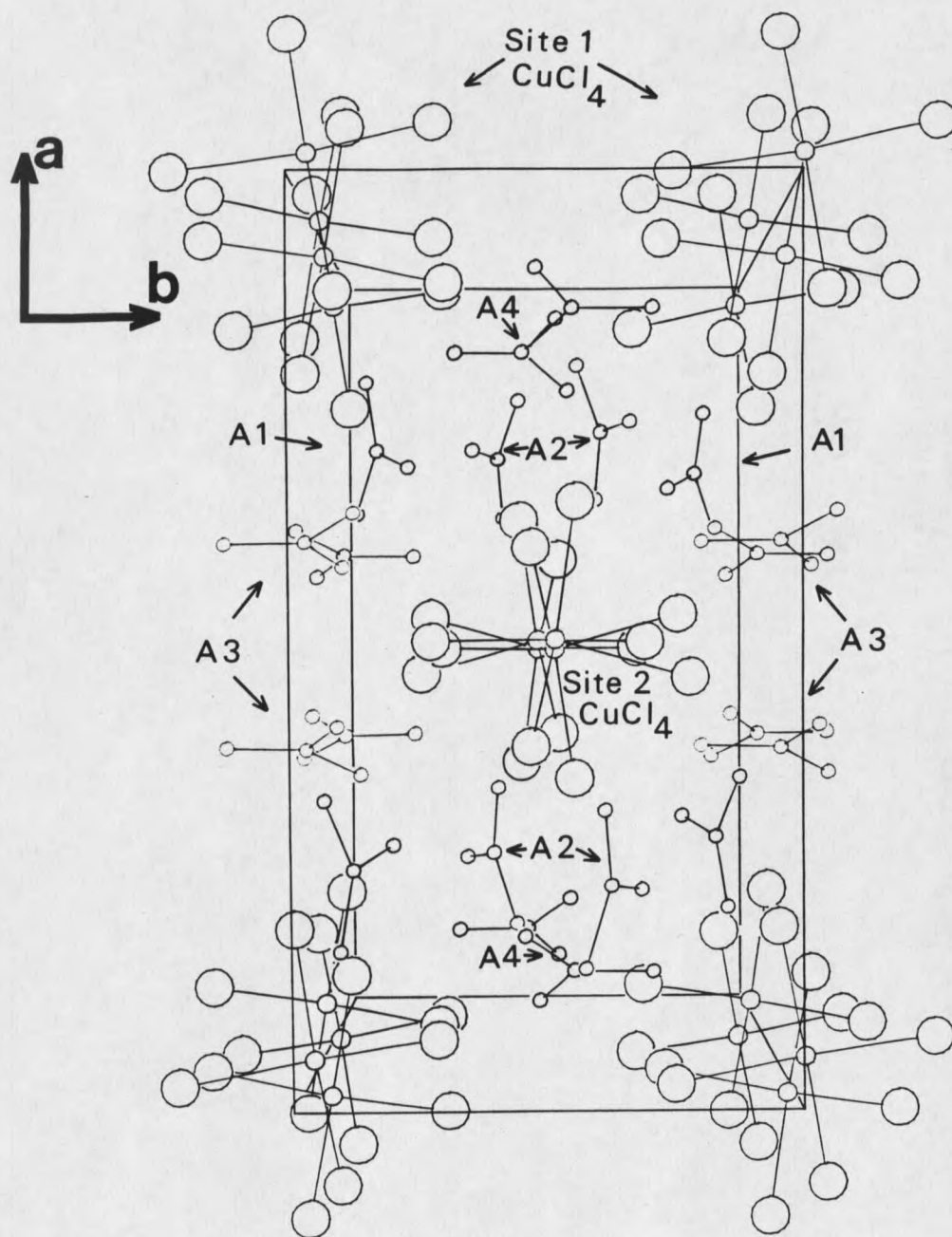


Figure 11. A three dimension representation of the unit cell of AceTCC projected onto the *a-b* plane. For clarity, hydrogen bonds are not shown. This perspective gives an edge-on view of the alternating *b-c* planes containing site 1 and site 2 CuCl_4 ions. The A4 and A3 groups link the chains into sheets coincident to the *a-b* plane and act as a weak bridge between the *b-c* planes.

CHAPTER FOUR

RESULTS AND DISCUSSION

Susceptibility Versus Temperature

Magnetic susceptibility measurements made over an extended range of temperatures provide a valuable means for diagnosing the magnetic properties of a given substance. Figure 12 shows a typical temperature scan for a single crystal of AceTCC taken at a constant field strength of 4.5kOe. The sample was oriented so that the magnetic field was perpendicular to the principle crystallographic face. The resulting characteristic plot identifies AceTCC as an antiferromagnet with a Neel temperature $T_N = 2.5K$ at 4.5kOe. Above the Neel temperature the magnetic susceptibility has a temperature dependence characterized by the Curie-Weiss law.

The plot of inverse susceptibility against temperature is given in Figure 13 and shows the data following a straight line above T_N which extrapolates to a negative value at the temperature, $\theta = -1.6K$. Measurement of the slope shows the Curie-Weiss constant, C , to equal 0.33 (moles/emu.K). From molecular field theory, θ is a measure of the interaction strength between magnetic moments. The negative θ indicates a negative exchange force characteristic of antiferromagnets. The physical significance is that below T_N , for a simple two-sublattice antiferromagnet, adjacent moments tend to align

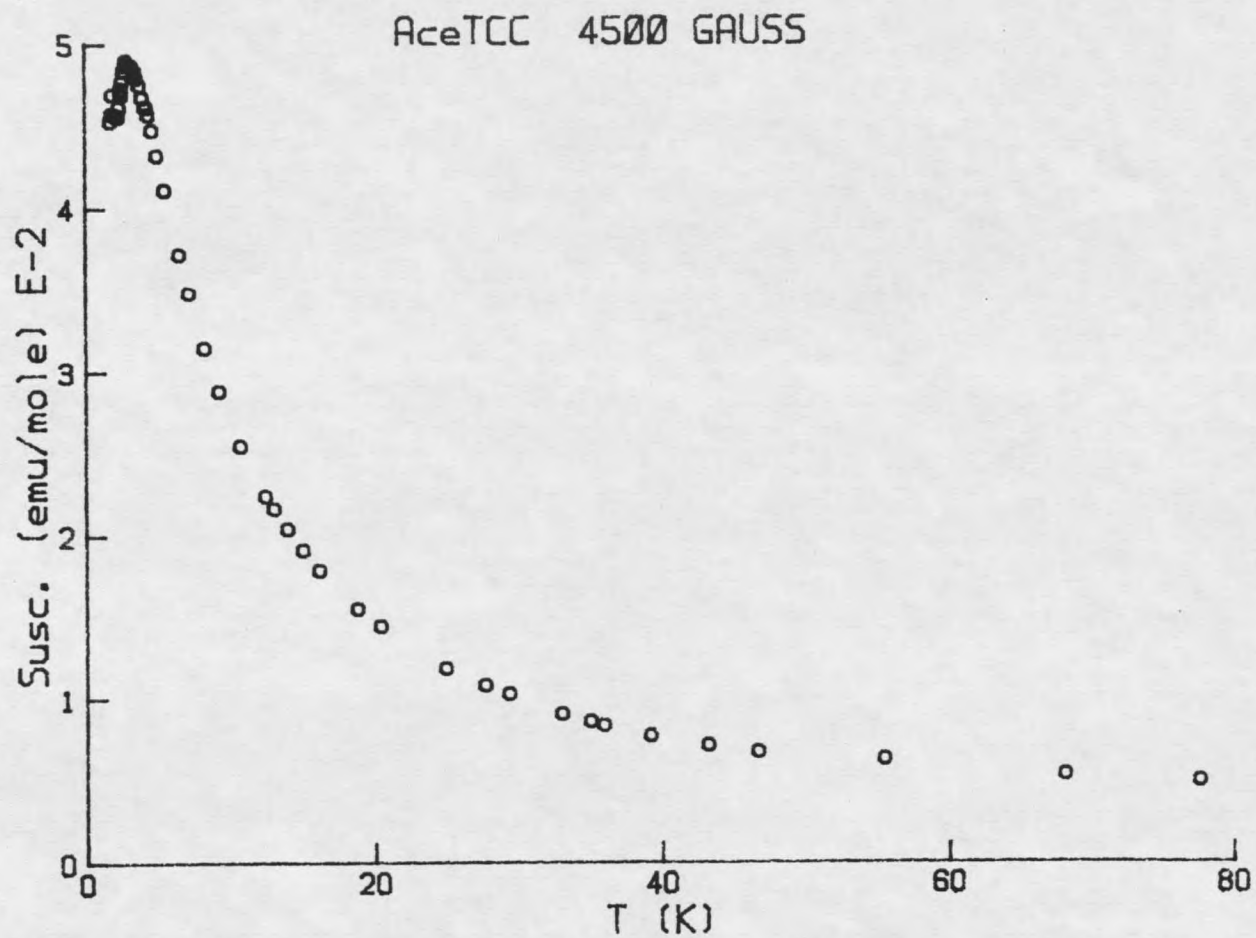


Figure 12. Susceptibility of AceTCC versus temperature at a field strength of 4500 Gauss. Measurement was taken along the a-axis.

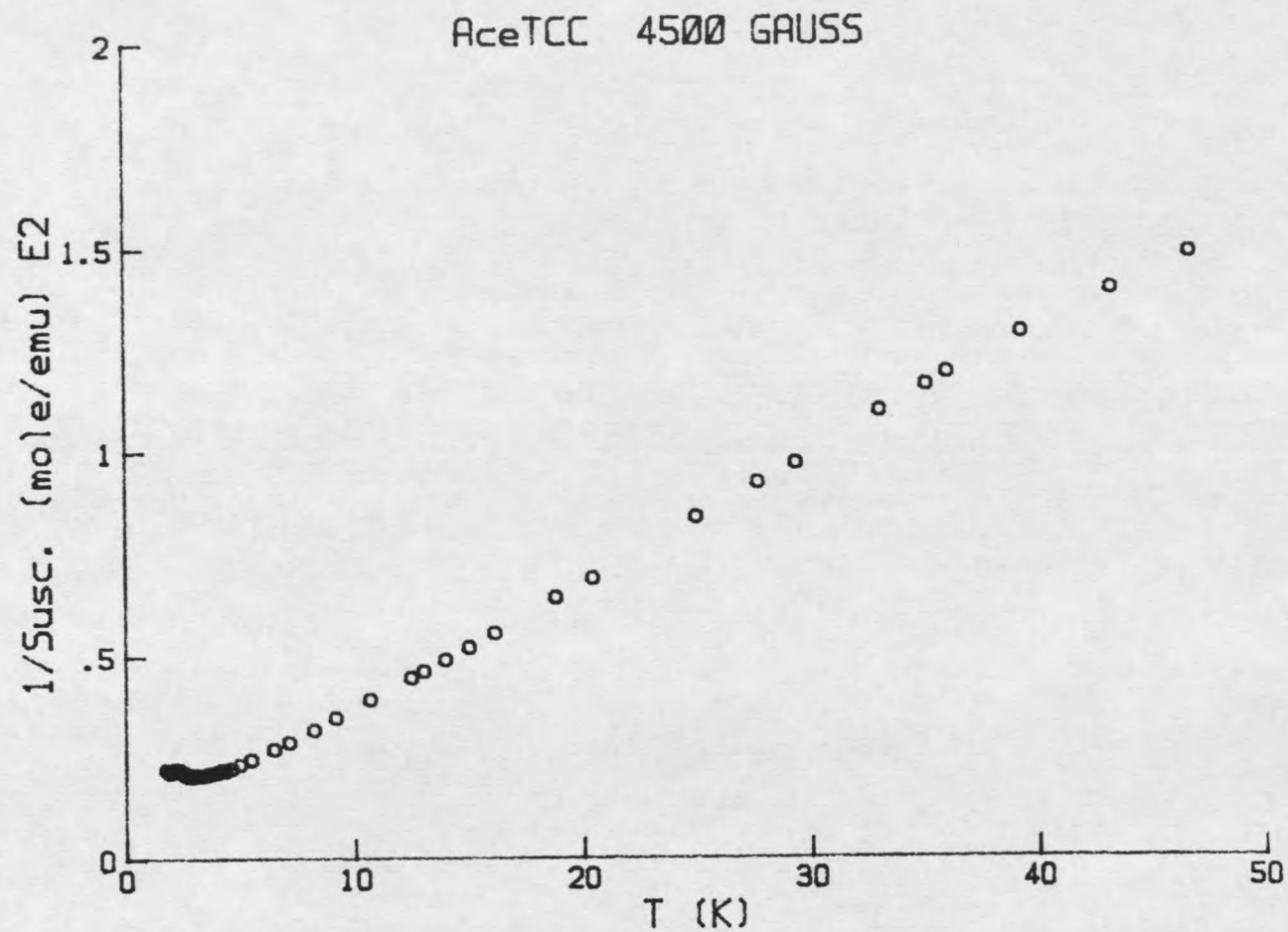


Figure 13. Inverse susceptibility versus temperature at a field strength of 4500 Gauss applied parallel to the a-axis.

antiparallel to one another. However, evidence presented below suggests that AceTCC is not a typical two-sublattice antiferromagnet.

An expanded view of the transition area is provided in Figure 14 and reveals evidence for two distinct peaks at 2.5K and 1.8K, suggesting the interesting possibility of two phase transitions instead of one. This unexpected double peak is observed in all of the temperature scans shown in Figures 27 through 29 of the appendix. Evidence of two transitions in antiferromagnets is rare. Consequently, the interpretations are speculative and a part of on-going research.

One possible interpretation is that there are two distinct pairs of interpenetrating sublattices each of which, having different exchange energies, tend to order at slightly different temperatures. Above 2.5K the system behaves paramagnetically as the effects of thermal agitation dominate and favor random orientation of all the magnetic moments. However, as the temperature is lowered, the exchange interactions between magnetic ions of one set of sublattices begin to compete with the diminishing thermal energies, allowing the pair of sublattices with the stronger exchange path to order at a slightly higher temperature. This ordering can only occur because of three dimensional fluctuations which include the non-ordered sublattice. The fact that the peak occurring at 2.5K is much broader than the peak at 1.8K tends to suggest one dimensional ordering along linear chains comprising the one pair of sublattices. As the temperature continues to decrease, the remaining sublattice pair orders, completing the three dimensional ordering of the system. This latter transition would correspond to the sharper peak at 1.8K.

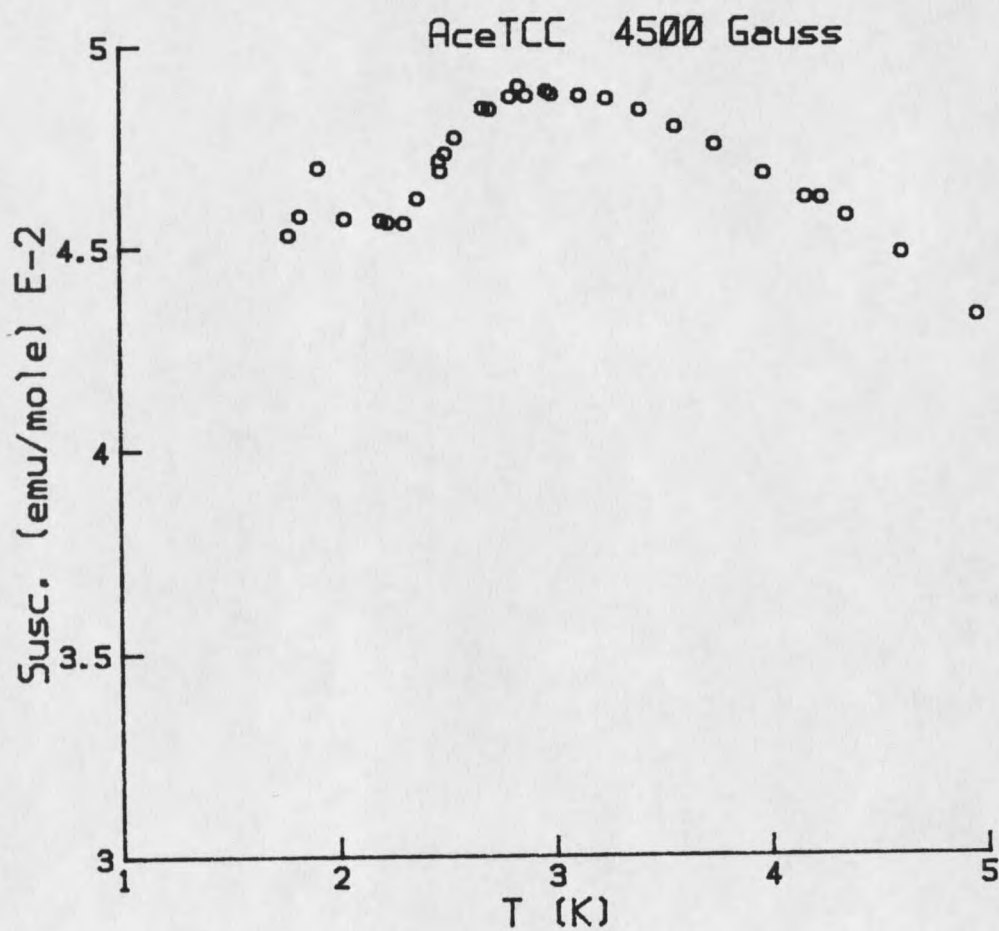


Figure 14. Expanded view of the transition area seen in figure 11. Two separate peaks in the susceptibility are revealed corresponding to Neel temperatures of 2.5K and 1.8K.

Magnetization Versus Angle and Field

Magnetic measurements were performed on single crystals in fields up to 5.5kOe for different temperatures and crystallographic directions. From these measurements an attempt was made to determine the spin-flop field and direction of the easy axis.

In the ordered state the magnetic spins of a sample are bound tightly in an antiferromagnetic configuration along the easy axis. Consequently, the direction of easy spin alignment corresponds to a minimum in magnetization. Magnetization versus crystal orientation was observed at a temperature below T_N and in fields just below the spin-flop field. For orientations corresponding to a minimum in magnetization, a magnetic field scan was performed to determine the presence or absence of an easy axis. The presence of an easy axis along the direction of the applied field is determined conclusively if the magnetic field scan results in a characteristic spin-flop curve similar to that shown previously in Figure 6.

A single crystal of AceTCC was rotated about the 'needle' axis which runs parallel to the b-axis shown in the coordinate system defined in Figure 15. The resulting angle scan presented in Figure 16 discloses a minimum magnetization for the angles $\phi = 90^\circ$ and $\phi = 270^\circ$, both of which correspond to a field applied along the a-axis. Magnetization versus field was observed at 1.75K for a field direction coincident to the a-axis. The resulting scan shown in Figure 17 reveals no evidence for a spin-flop transition, however, an interesting jump in magnetization occurring at 2.6kOe suggests the

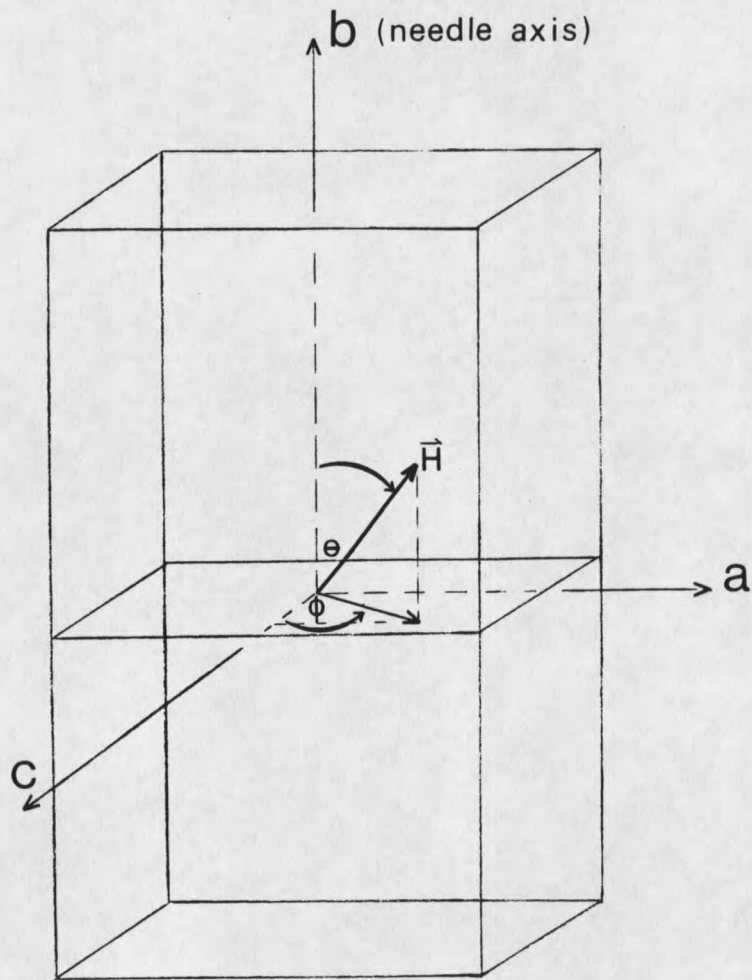


Figure 15. Laboratory coordinate system describing the orientation of an AceTCC crystal in an applied magnetic field, H .

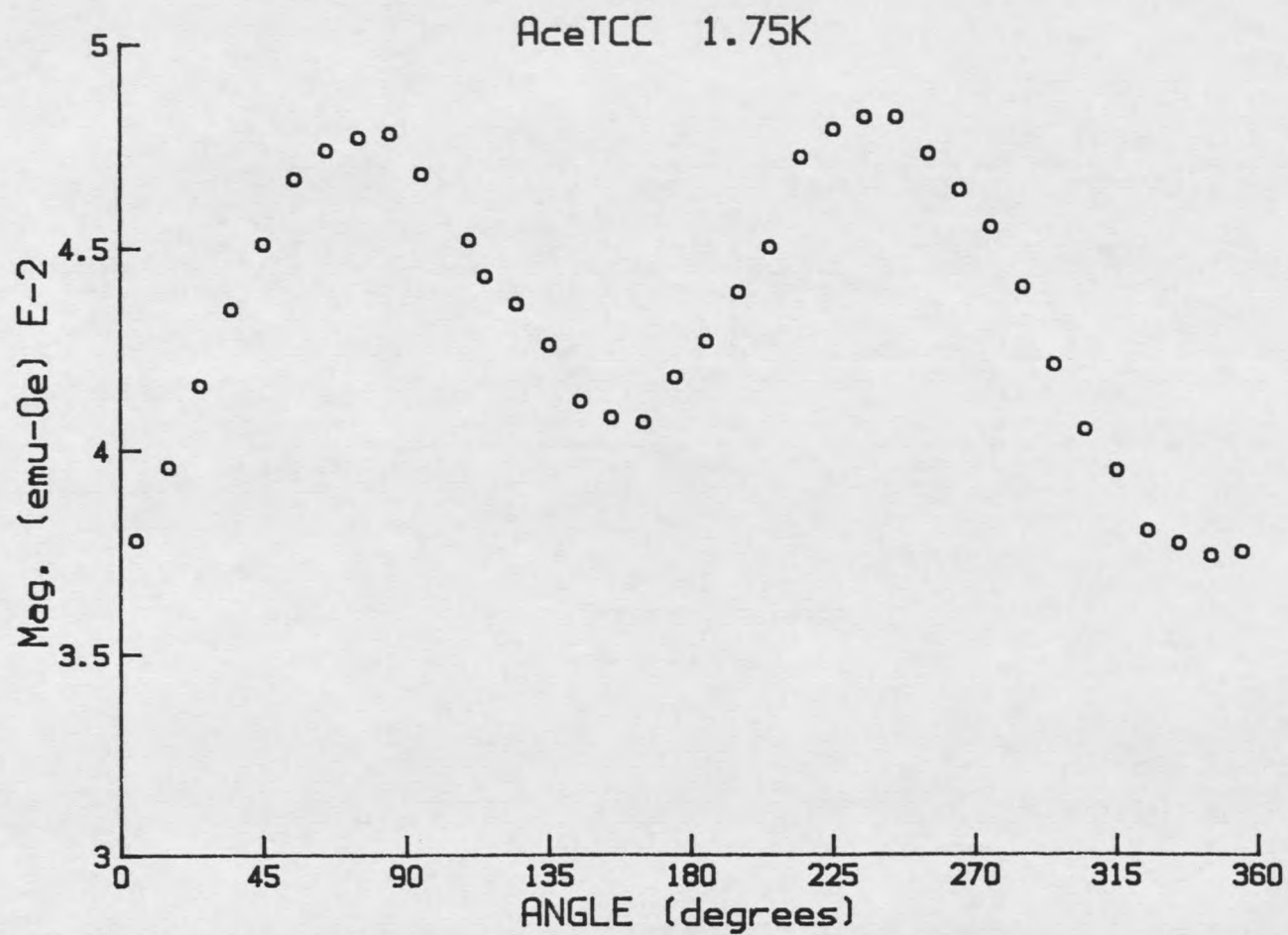


Figure 16. Angle dependence of magnetization of AceTCC in the a-c plane at 1.75K ($\theta = 90^\circ$; $\phi = 0^\circ-360^\circ$).

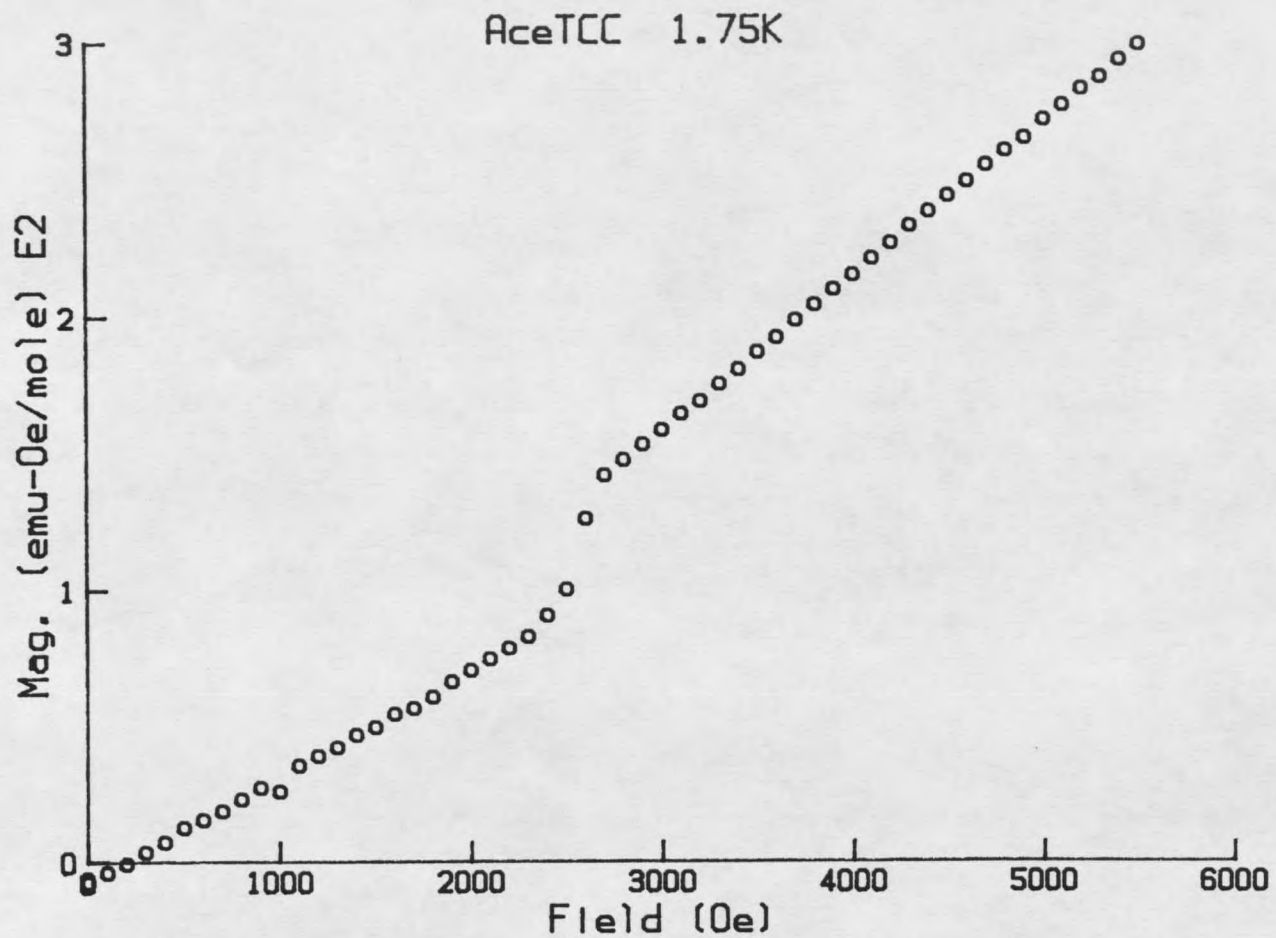


Figure 17. Magnetization versus field at 1.75K. Measurements were taken with H applied parallel to the a-axis.

unexpected possibility of a magneto-structural phase transition occurring at this field strength.

This discontinuity occurs consistently in further scans performed in the a-c plane at angles $\phi = 20^\circ$ and $\phi = 45^\circ$. The corresponding results are provided in Figures 18 and 19 respectively. The lack of evidence for a spin-flop transition in any of the above field scans indicates that if an easy axis exists it is most likely outside of the a-c plane. The search for an easy axis in the other two principle planes was hampered by extremely weak signals due to restrictions placed on the sample size which the VSM will accommodate. In order to observe in either the a-b or b-c plane, the crystal had to be reduced in size by about 75%, leading to a drastically reduced signal intensity barely discernible from background noise.

Although the search for an easy axis proved unsuccessful, supporting evidence for a structural phase transition was obtained via additional field scans. At a fixed crystal orientation of $\phi = 0^\circ$, field scans were obtained in the a-c plane for three different temperatures, 1.75K, 1.9K and 3K with results shown in Figures 20 through 22 respectively. The three temperatures were chosen to include a temperature below and above the two Neel temperatures and one directly in between. The results show that the discontinuity disappears at a temperature just above the higher Neel temperature, indicating that the transition to an ordered state may trigger an energy exchange resulting in the structural phase transition. To further exclude the possibility of any contributing effects due to the crystallographic orientation of the sample, magnetic field scans were

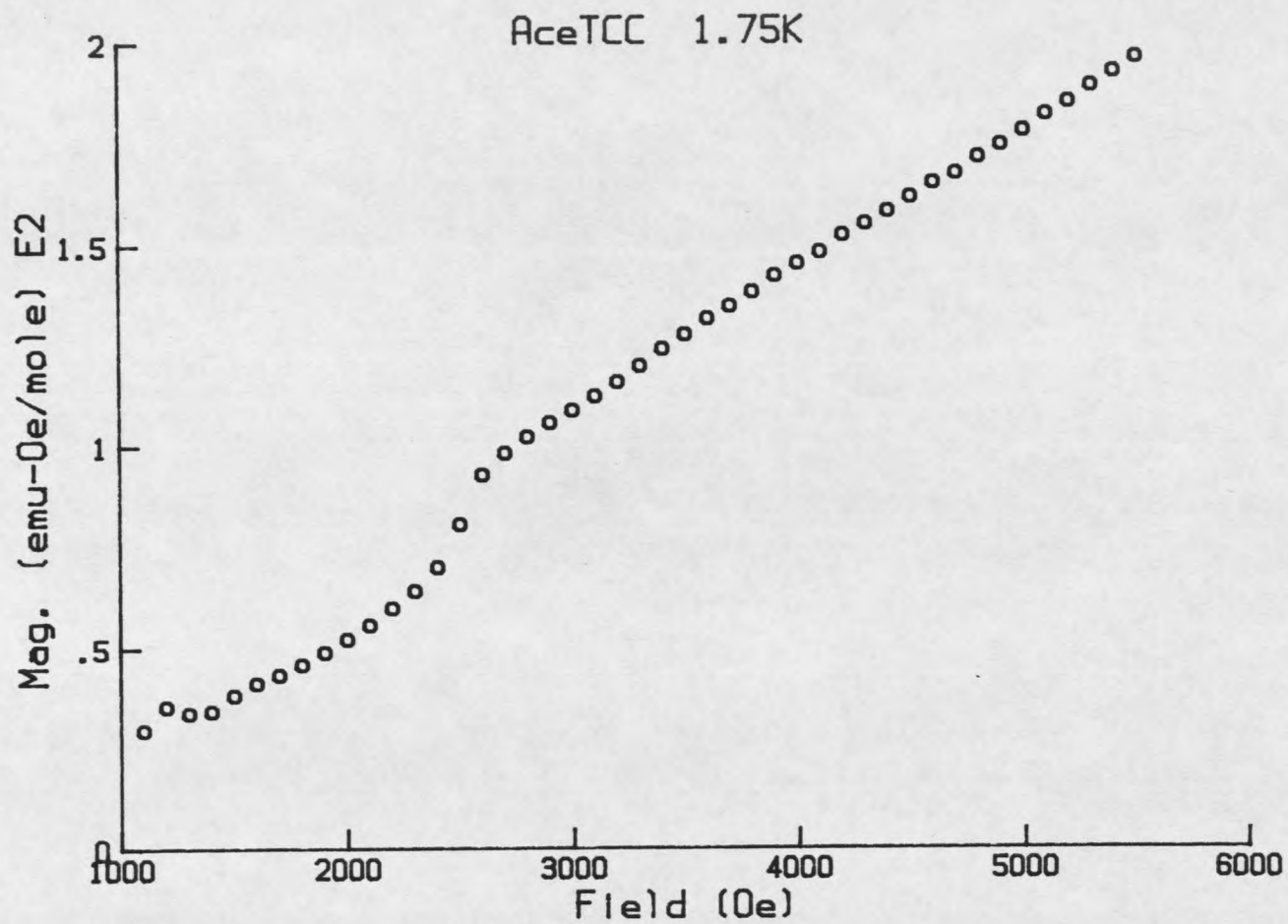


Figure 18. Magnetization versus field at 1.75K with $\theta = 90^\circ$ and $\phi = 20^\circ$.

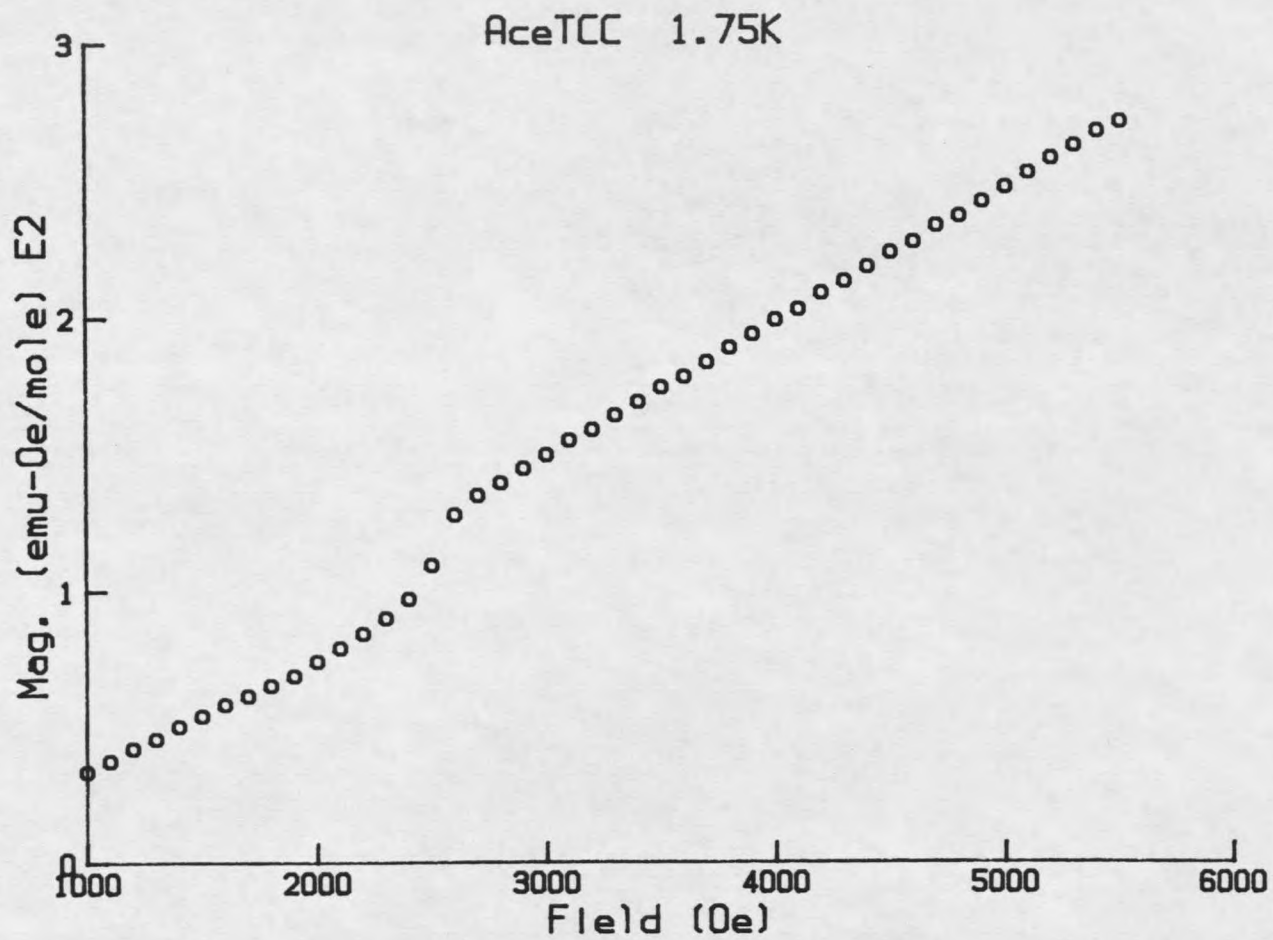


Figure 19. Magnetization versus field at 1.75K with $\theta = 90^\circ$ and $\phi = 45^\circ$.

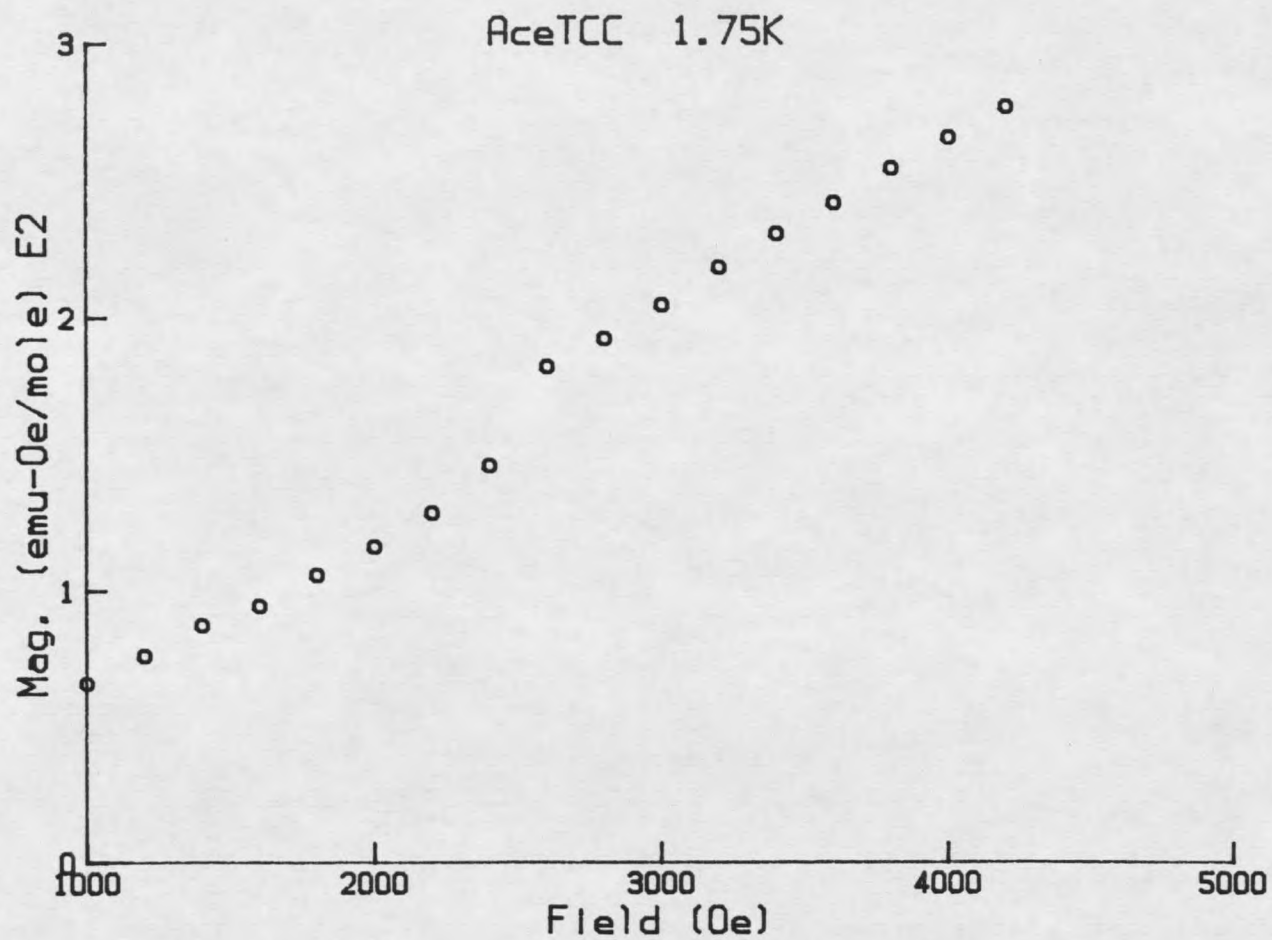


Figure 20. Magnetization versus field at 1.75K with $\theta = 90^\circ$ and $\phi = 0^\circ$ (H coincident to the c-axis).

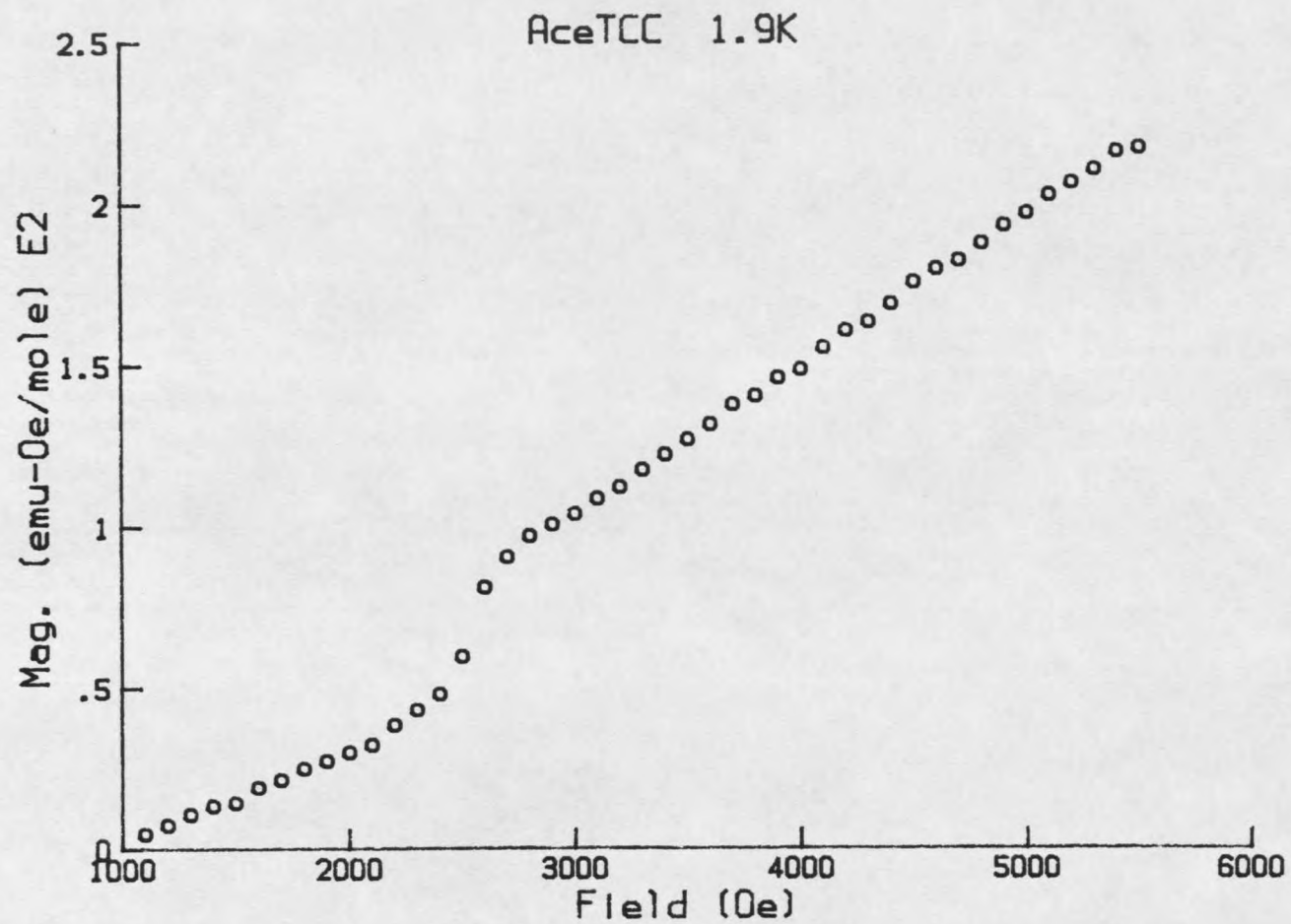


Figure 21. Magnetization versus field at 1.9K with $\theta = 90^\circ$ and $\phi = 0^\circ$ (H coincident to the c-axis).

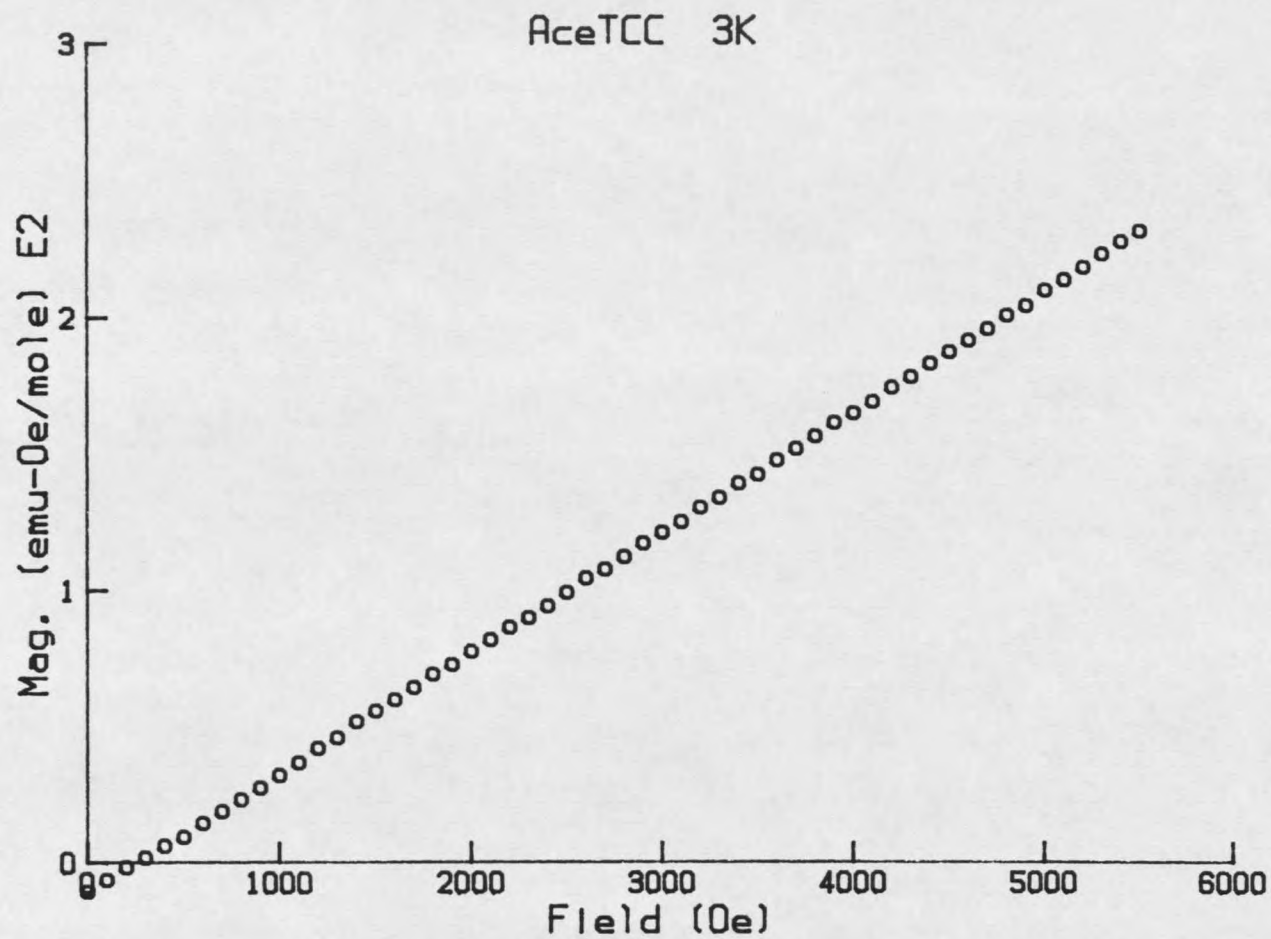


Figure 22. Magnetization versus field at 3K with $\theta = 90^\circ$ and $\phi = 0^\circ$ (H coincident to the c-axis).

also taken at the same three temperatures for a powdered sample. Consistent with the above results, the discontinuity appears at sub-transition temperatures, 1.75K and 1.9K, but disappears again above the transition temperature at $T = 3K$ as shown in Figures 23 and 24.

It should be pointed out that although the easy axis indicates a minimum signal, the converse is not necessarily true. Superimposed on the angle dependence study is the existing anisotropy in the Lande g -factor. If the easy axis happens to lie outside the plane of rotation, the g -factor anisotropy will be the primary source of any angle dependence observed in the magnetization. Therefore, the absence of evidence for a spin-flop curve in the a - c plane suggests that the minimum observed in the magnetization versus crystal orientation data of Figure 16 coincides with a minimum in the Lande g -factor.

Comparison with EPR Study

This measured anisotropy is confirmed by EPR (electron paramagnetic resonance) measurements recently reported by Wan (in prep). In addition, Wan cites a critical linewidth broadening of two separate resonances at the two Neel temperatures reported in this study. This is consistent with the proposed interpretation of two distinct pairs of sublattices, each characterized by slightly different exchange constants J . EPR techniques also enable the effective value of g to be calculated. Results provided by Wan assign the following values to the g tensor elements:

$$g_{xx} = 2.1$$

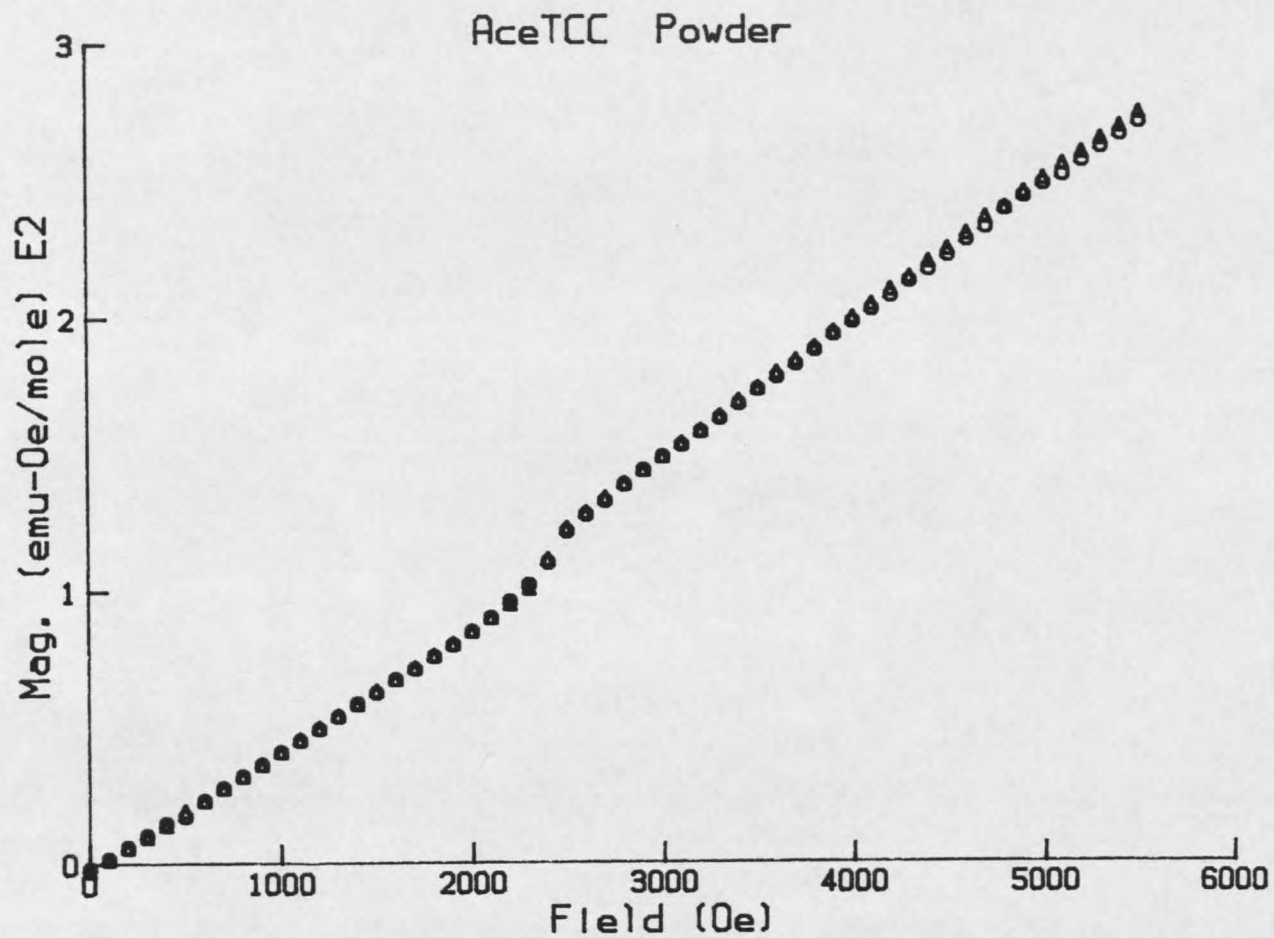


Figure 23. Magnetization versus field for a powder sample of AceTCC. Circles and triangles correspond to measurements taken at 1.75K and 1.9K, respectively.

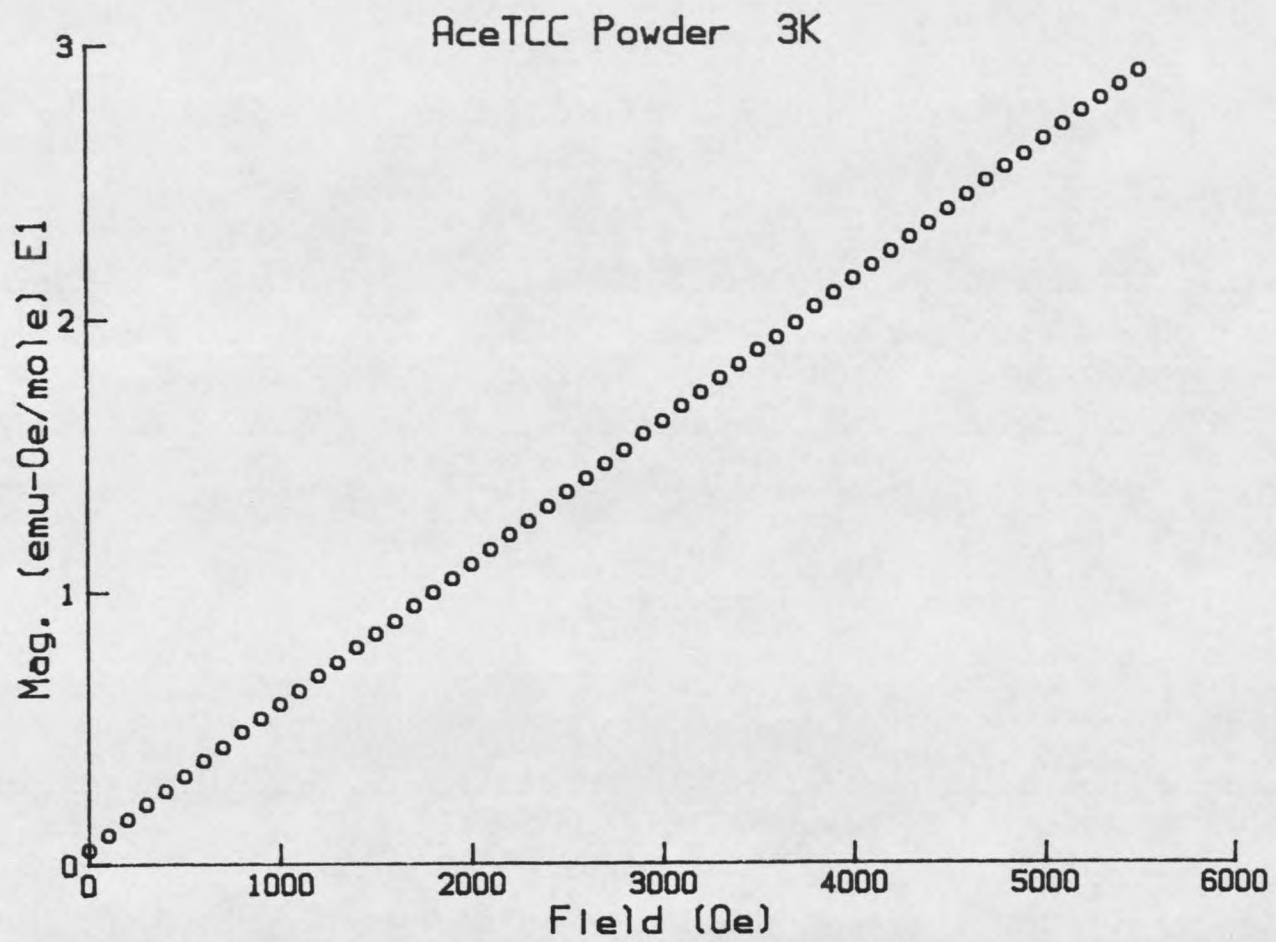


Figure 24. Magnetization versus field for a powder sample of AceTCC at 3K.

$$\begin{aligned}g_{yy} &= 2.1 \\g_{zz} &= 2.4,\end{aligned}$$

with near-zero values for the off-diagonal elements. These measured g values have been used in this study to determine a numerical estimate of the exchange parameter J .

High Temperature Series Expansion

A high temperature series expansion of the partition function for the spin 1/2 Heisenberg model was applied as a three-parameter model fit to magnetic susceptibility data. Results yield an estimated Curie constant of 0.31 (moles/emu.K) which corresponds to a relative error of 6% with respect to the measured value of 0.33 (moles/emu.K). Although the series fails to converge at temperatures very near the Neel temperature, it converges rapidly at higher temperatures and thus provides sufficient accuracy with only five leading terms. Figure 25 presents the best fit corresponding to a standard deviation of 8.21×10^{-5} with $J_1/k = 0.66K$ and $J_2/k = -2.15K$. From the constructs of the theoretical model, J_2 represents an exchange energy directed along linear chains, while J_1 represents an exchange energy between chains. Any exchange, J_3 , which might occur between planes is very weak and is not measurable by the high temperature series expansion method. From the estimated values of J_1 and J_2 , it is possible to deduce an anti-ferromagnetic exchange coupling along chains of magnetic Cu^{++} sites. A much weaker intra-planar ferromagnetic coupling occurs between the chains, connecting the chains into sheets.

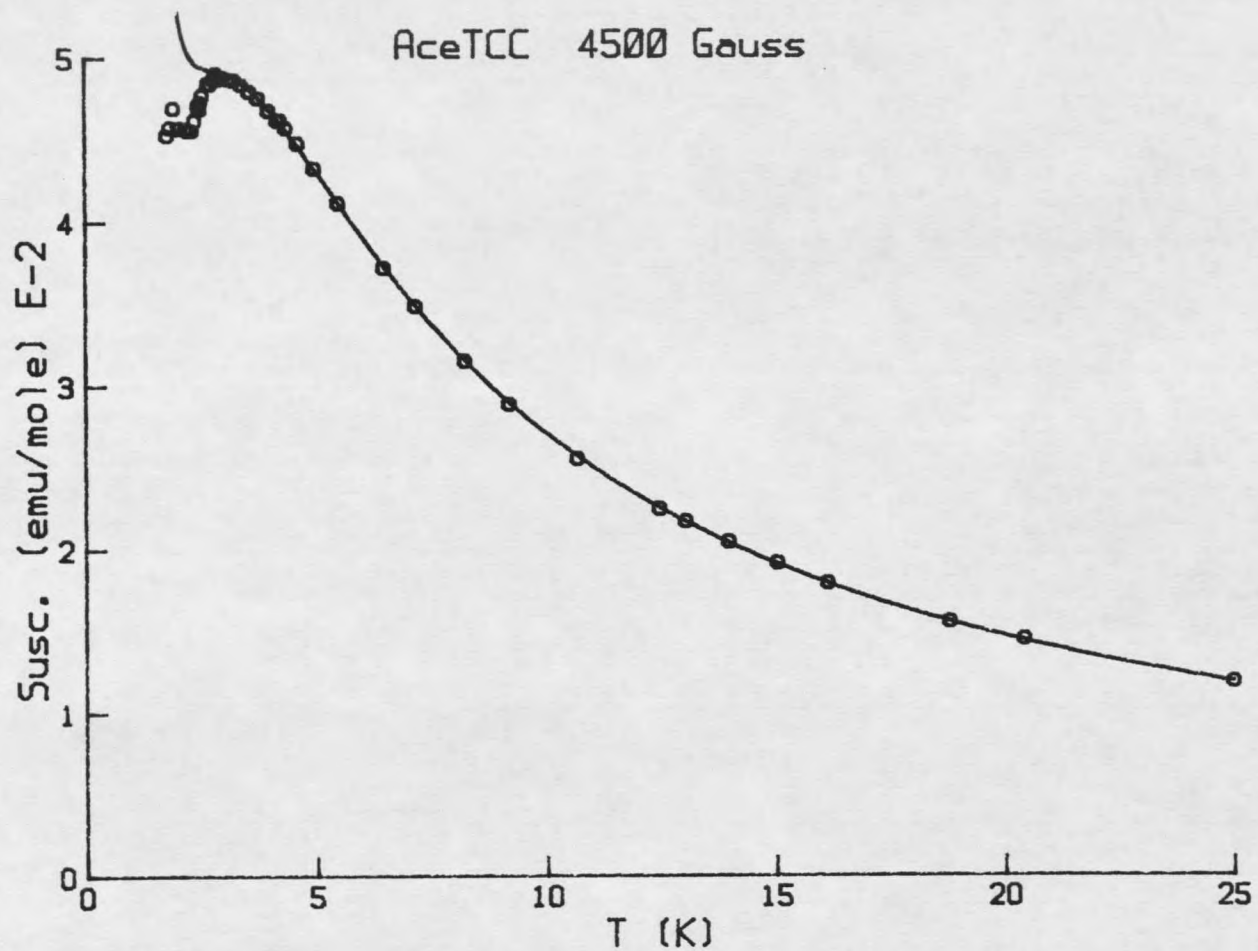


Figure 25. Magnetic susceptibility data (circles) fitted to a theoretical high temperature series expansion of susceptibility for a spin 1/2 Heisenberg interaction.

Comparison with Crystallographic Data

Crystallographic data reported by Emerson, et al. (in press) indicate that the layers are formed by two crystallographically distinct distorted tetrahedral CuCl_4 groups linked into inequivalent chains by intermediate acetamidinium ions. These nonmagnetic acetamidinium ions form an indirect path through which the strongest exchange, J_2 , occurs. This results in an antiferromagnetic ordering of Cu^{++} magnetic moments along chains parallel to the b-axis. A network of hydrogen bonds parallel to the crystallographic c-axis connects the chains so that they form sheets coincident to the b-c plane. These bonds act as an indirect path for a weak ferromagnetic exchange interaction, $J_1/k = 0.66\text{K}$, between chains as shown schematically in Figure 26.

One can assume that two distinct exchange interactions, J_2 and J_2' , exist which link the two crystallographically distinct CuCl_4 sites into separate chains. Unfortunately, the model used in this study, as well as any model currently available, fails to distinguish between J_2 and J_2' . However, the evidence of a double transition in the susceptibility versus Temperature scans suggest that J_2 and J_2' are slightly different. This is consistent with the interpretation of two distinct interpenetrating sublattice pairs AB and CD, each of which having different exchange energies, tend to order at slightly different temperatures. The cited value for J_2 is an average of the antiferromagnetic exchange constants contributed by both sublattice pairs.

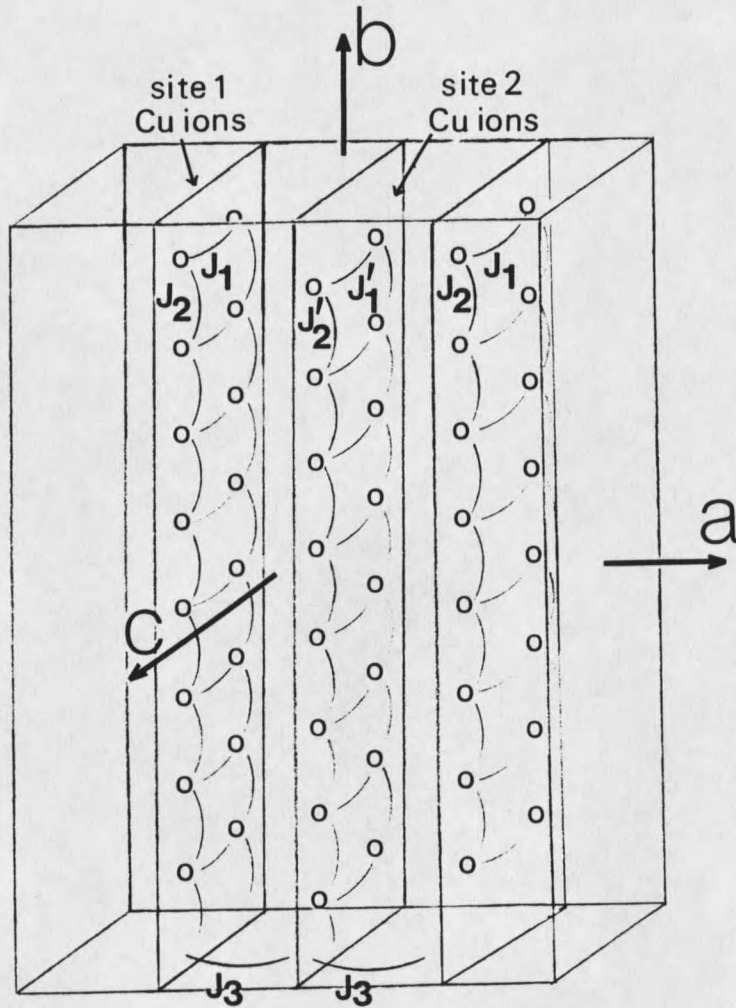


Figure 26. A schematic representation of AceTCC showing sheets of site 1 and site 2 copper ions coincident to the b-c plane. One dimensional antiferromagnetic exchange interactions, J_2 and J_2' , occur along chains parallel to the b-axis. Weaker ferromagnetic exchange interactions, J_1 and J_1' link the chains into sheets. It is assumed that an even weaker inter-planar exchange, J_3 , serves as a bridge between the b-c planes.

Crystallographic data indicates that the weaker ferromagnetic exchange coupling, J_1 , serves as a bridge connecting the two inequivalent chains into parallel sheets coincident to the b-c plane. Because the dominant exchange is antiferromagnetic and acts linearly along chains of magnetic Cu^{++} ions, the system is described as a weak pseudo one-dimensional, spin 1/2 Heisenberg antiferromagnet.

CHAPTER V

CONCLUSIONS

The results of this study show that the tetrahedrally coordinated system, AceTCC, can be characterized as a pseudo one dimensional spin $1/2$ Heisenberg antiferromagnet. Two distinct peaks at 2.5K and 1.8K occur in the magnetic susceptibility which suggest the possibility of two phase transitions corresponding to antiferromagnetic ordering of two different sublattice pairs. These sublattice pairs are formed by two crystallographically distinct tetrahedral CuCl_4 groups linked into chains parallel to the b-axis by intermediate acetamidinium ions. Data were fitted to a high temperature series expansion and an exchange interaction, $J_2 = -2.15\text{K}$, was found to occur between magnetic ions, causing antiferromagnetic ordering along these two inequivalent systems of chains. A weaker ferromagnetic exchange interaction links the chains into planes coincident to the b-c plane. It is proposed that these two inequivalent chains form a unique four sublattice system in which one set of chains order throughout the crystal at 2.5K, followed by a three dimensional ordering at 1.8K. This interpretation is consistent with critical EPR linewidth broadening of two separate resonances at the two cited transition temperatures. Although evidence for an easy axis was not found, this study does reveal evidence for the occurrence of a magneto-structural phase transition

at 2600 Oe. As of yet, the mechanism for this magneto-structural transition is unexplained.

To date, only a few studies of tetrahedrally coordinated systems have been attempted. Hence, many important questions concerning the magnetic properties of these poorly understood systems remain. It is hoped that further work will instigate the synthesis and characterization of new chemical analogs to AcTCC .

REFERENCES CITED

- Bares, L. A., Emerson, K., and Drumheller, J. E., *Inorganic Chemistry* 8, 131 (1969).
- Cullity, B. D. Introduction to Magnetic Materials, Addison-Wesley Publishing Co. (1972).
- Dirac, P. A. M. *Proc. Roy. Soc. Ser. A*112, 661 (1926).
- Domb, C. and Sykes, M. F. *Phys. Rev.*, 128, 168 (1962).
- Emerson, K., Pressprich, M., Nilsen, D., Drumheller, J. E., Olsen, R., Witters, R., *Inorganic Chem.* (Submitted, 1987).
- Fishes, M. E. *Phil. Mag.* 7, 1731 (1962).
- Haines, D. N. and Drumheller, J. E., *Phys. Rev. Letters*, 58, 2702 (1987).
- Heisenberg, W. *Z. Physik* 38, 411 (1926); 49, 619 (1928).
- Hoogerbeets, R., van Duyneveldt, A. J., Phaff, A. C., Swuste, W., and de Jonge, W. J. M., *J. Phys. C* 17, 2595 (1984).
- Kittel, C. Elementary Statistical Physics, Wiley (1958).
- Kubo, R. *Phys. Rev.*, 87, 568 (1952).
- Lasheen, M. A., Van Den Broek, J., and Gorter, C. J., *Physica*, 24, 1061 (1958).
- Martin, D. H., Magnetism in Solids, M. I. T. Press (1967).
- Nagamiya, *Progr. Theort. Phys. (Kyoto)* 6, 342 (1951).
- Newell, G. E. and Montroll, E. W. *Revs. Mod. Phys.* 25, 353 (1953)
- Opechowski, W. *Physica*, 4, 181 (1937); 6, 1112 (1938).
- Rushbrooke, G. S. and Wood, P. J. *Mol. Phys.*, 1, 257 (1958).
- Van Dongan, E. J., Capel, H. W. and Siskin, T. J., *Physica A*, 79, 617 (1975).
- Van Vleck, J. H., *J. Chem. Phys.* 9, 85 (1941).
- Weiss, P. J. *Phys. Radium* 4, 661 (1907).

APPENDIX

Supplemental Susceptibility Plots

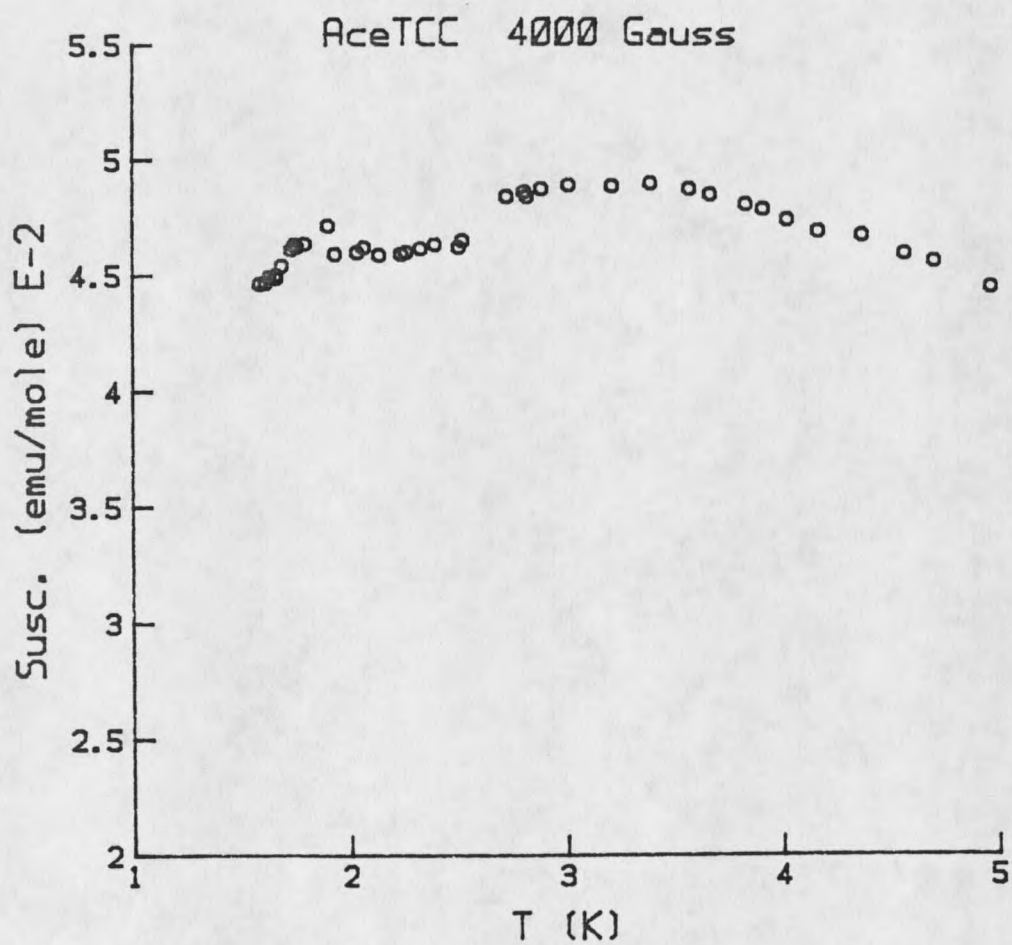


Figure 27. Expanded view of the transition area of a susceptibility versus temperature scan. Measurements were taken at a constant field strength of 4000 Gauss.

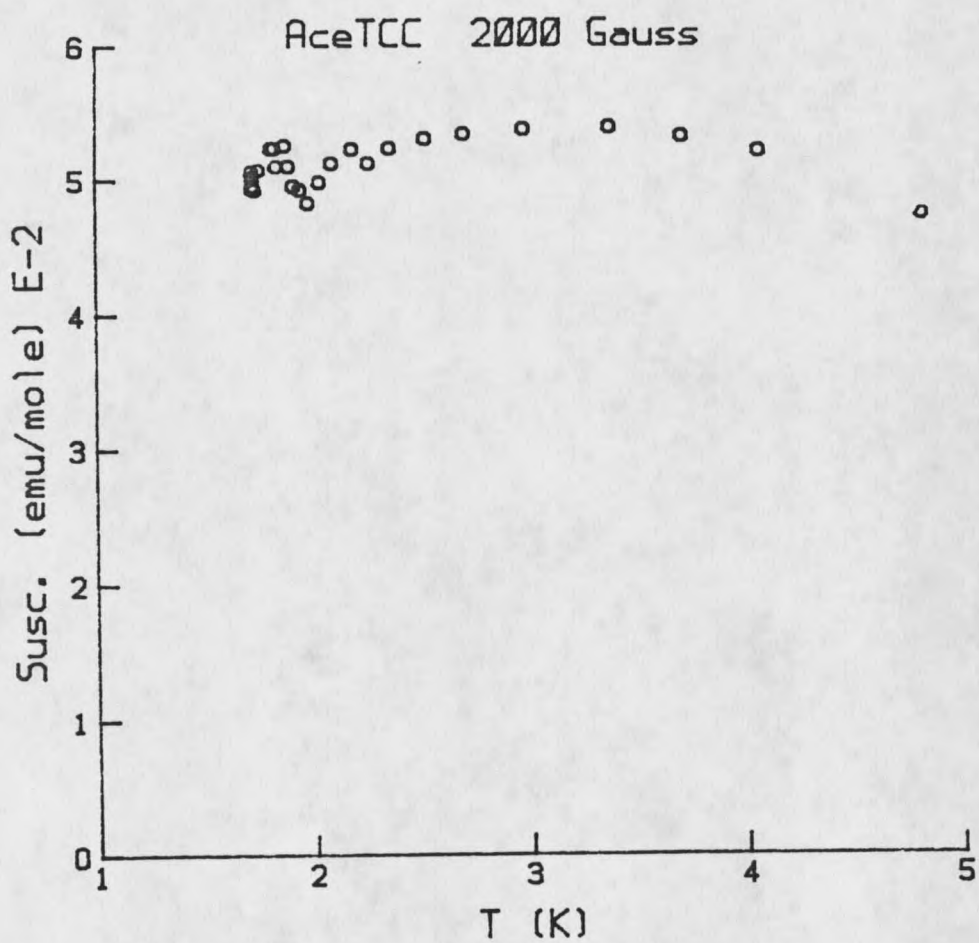


Figure 28. Expanded view of the transition area of a susceptibility versus temperature scan. Measurements were taken at a constant field strength of 2000 Gauss.

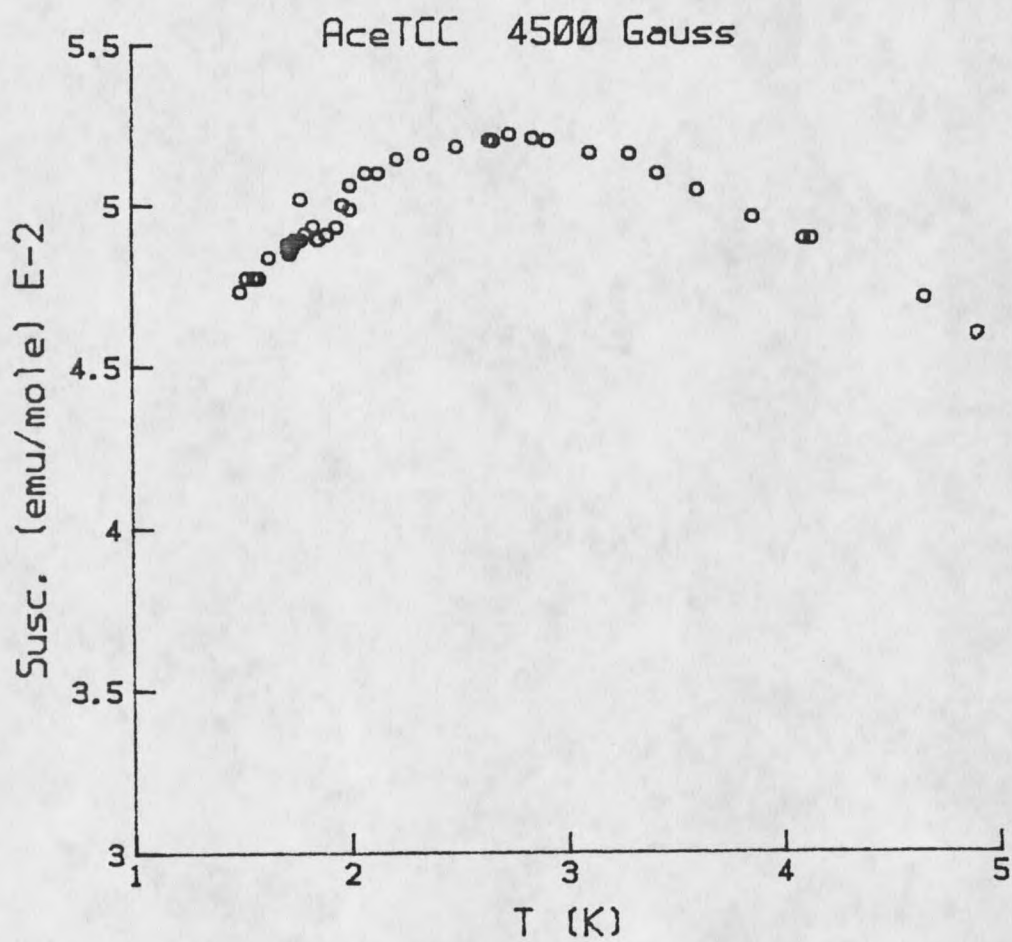


Figure 29. Expanded view of the transition area of a susceptibility versus temperature scan. Measurements were taken at a constant field strength of 4500 Gauss.

MONTANA STATE UNIVERSITY LIBRARIES



3 1762 10024282 3

